

Breaking of shape symmetries in heavy nuclei in regard of electro-magnetic strength, level density and radiative capture

E. Grosse, A.R. Junghans, and R. Massarczyk¹,

Institute of Nuclear and Particle Physics, Technische Universität Dresden,
01062 Dresden, Germany

and

Institute of Radiation Physics,
Helmholtz-Zentrum Dresden-Rossendorf, 01314 Dresden, Germany

Triggered by a recent prediction of broken axial symmetry in most heavy nuclei a systematic review of data is presented, which were previously analysed assuming axiality, namely the splitting of giant dipole resonances (GDR) as well as resonance spacings just above the neutron threshold. It will be shown, that a modified interpretation of both has an important effect on the prediction of radiative processes including neutron capture in the energy range of unresolved resonances. The theoretical predictions were based on a constrained HFB calculation with the Gogny D1S interaction and their validity is tested via comparison to multiple Coulomb excitation results explicitly examining axial deformation and triaxiality. For GDR shapes a parameterization by the sum of three Lorentzians (TLO) results; level densities are influenced strongly by the significant collective enhancement based on the breaking of axiality. In both cases the replacement of axial symmetry by the less stringent requirement of invariance against rotation by π (\mathcal{R}_π) leads to one global set of parameters for the full range in nuclear mass number A from 50 to 250, which is astonishingly small. The discussion on new modes adding to the low energy GDR slope is also reviewed including recent photon scattering experiments and other photonic processes. These are shown to be of minor importance e.g. for a comparison with experimental Maxwellian averaged cross sections for neutron capture by even target nuclei from Se to Cm, albeit only conventional methods are used for the parameterization of the GDR: In accordance to the dipole sum rule the droplet model with surface dissipation accounts well for their position and width without additional parameters. Thus a reliable prediction for compound nuclear reactions also outside the valley of stability is expected.

I. Introduction

The ongoing discussion [de10, ok12, ni12, wr12, to13] about triaxial shapes in heavy nuclei, often newly studied or far off stability, may induce the question, how well the widely used assumption about axial symmetry of most less exotic nuclei is founded on sufficiently sensitive experimental data. Here conclusions from masses and level energies seem to be not very conclusive, whereas the splitting of the Isovector Giant Dipole Resonance (IVGDR) is an indicator which made it into text books – in spite of the need to adjust the apparent width locally for the five isotopes regarded [bo75]. In the present work this feature will be reviewed for 23 nuclei (as examples) in a wide range of mass number A under the assumption of broken axial symmetry; it allows a description with one global parameter only, which is valid for all nuclei regarded. A similar reduction is found for the other topic of this review, the accordance of capture resonance spacings to a Fermi gas prediction. Respective experimental information as obtained with more than 140 spin-0 target nuclei will be shown in this study to be influenced by broken axial shape symmetry. In a third, more introductory part, information from low energy nuclear structure studies in support of triaxiality will be presented. Experimental energy spectra have been interpreted in the past preferentially assuming at least

¹ present address: Los Alamos National Laboratory, Los Alamos, New Mexico 87545, USA

axial symmetry of the nuclear shape [al56, na65, bo57, bo75]. Similarly the well documented electromagnetic excitation of the lowest levels was considered as a measure of axial deformation only [ra01], although predictions of electromagnetic nuclear properties are clearly influenced by its breaking [ku72]. Here detailed studies of Coulomb excitation processes have investigated the influence of the details of nuclear shape symmetries and their breaking and results will be regarded in comparison to recent theoretical calculations [de10]. The common feature in the interpretation of the three experimental phenomena reviewed in the following is the replacement of the requirement of axiality by the less stringent assumption of invariance against rotation by an angle π , \mathcal{R}_π .

The paper will first review the various connections between nuclear shapes and electric quadrupole moments and transition rates; they have significantly affected our knowledge about fundamental nuclear properties as size and shape. After a short discussion of the importance of electromagnetic sum rules for the nuclear dipole strength, general features of the IVGDR as seen in photon reactions with heavy nuclei will be presented. In contrast to previous work a parameterization of the electric dipole strength is derived from IVGDR data without the usual *ad hoc* assumption about axial symmetry. This will be regarded with respect of its impact on the radiative capture process, for which the low energy behaviour of this strength is of major importance, as was noted recently for nuclei with mass number $A > 70$ [ju08]. The low energy tail of the electromagnetic dipole strength function depends sensitively on the proper description of the shape of the IVGDR, including not only its position, but also its width and substructure. In this report a parameterization of the dipole strength will be presented for heavy nuclei, which fully considers their triaxial deformation. Photon emission and absorption data are important here [ax70, ba73, gr12, he10, kn06, sa13] as they also may deliver information on the possible influence of other multipolarities. In a second part the influence of nuclear shape symmetry on the level density will be regarded, which strongly influences the phase space for radiative neutron capture and hence the size of the cross section for this important process. The radiative capture of fast neutrons by heavier nuclei plays an important role in considerations for advanced nuclear systems [ro57, ch06, sa11] and devices aiming for the transmutation of radioactive nuclear waste. This process is of interest also for the cosmic nucleosynthesis, especially for scenarios with such high fluxes of neutrons, that their capture becomes the main production process to reach heavier nuclides beyond Fe [bu57, ka89]. As the experimental studies which are the basis for respective predictions can be performed on nuclei in or close to the valley of beta-stability, the small number of global parameters increases their reliability.

II. Nuclear quadrupole moments and deformation

The electromagnetic response of nuclei has played an important role for the exploration of the size of nuclei and the departure of their shape from spherical symmetry was first indicated by a splitting of atomic transitions due to the nuclear electromagnetic field [sc35]. Much improved and accurate hyperfine structure measurements, partly using laser techniques, determined the ‘spectroscopic’ electric quadrupole ($\lambda=2$) moment Q_s of the ground state [st05] in nearly 800 odd nuclei. In addition, the reorientation effect in Coulomb excitation as well as muonic X-ray data Q_s -values became available for even and odd nuclei. In many cases the

sizes and signs – positive and negative values are observed – of these quadrupole moments were not in agreement to predictions for single particle or hole configurations [bo75]. In even nuclei, Coulomb excitation-reorientation data can yield ‘spectroscopic’ quadrupole moments for excited 2^+ -states $Q_s(2^+)$, and these were compiled [st05] for nearly 200 isotopes. If the sign of $Q_s(2^+)$ was determined, it mostly was negative indicating an oblate charge distribution in the laboratory system. A seemingly obvious picture [al56] interprets this as the result of the rotation of a deformed cigar like body with an ‘intrinsic’ quadrupole moment $Q_0 = -\frac{7}{2} Q_s(2^+)$ and an intrinsic prolate deformation for most even nuclei away from closed shells is suggested. The obviously much larger Q_0 values observed in lanthanide ($A \approx 170$) and actinide nuclei ($A \approx 240$) were seen as a strong indication for non-spherical nuclear shapes. Only for near magic isotopes like in the Os-Pt-Hg region positive $Q_s(2^+)$ were observed [sc35], indicating oblate intrinsic shapes, *i.e.* $Q_0 < 0$. Assuming axial symmetry and a homogeneous distribution of the charge within the nuclear volume, a rotational model was formulated, in which the intrinsic electric quadrupole moment Q_0 of even nuclei is related to the radius difference ΔR between the long and the two short axes of the shape by setting [al56]:

$$Q_0 \equiv \sqrt{\frac{9}{5\pi}} Z R^2 \beta (1 + b \cdot \beta); \quad \beta \cong \frac{4}{3} \sqrt{\frac{\pi}{5}} \frac{\Delta R}{R} \cong 1.057 \frac{\Delta R}{R} \quad (1)$$

The rotational model relation (1) between deformation β , Q_0 and ΔR is widely applied when electromagnetic data are related to calculated nuclear (mass) deformations usually characterized by β . For years $b \approx 0.16$ was often used [al56, da65], but later an often used compilation of electric quadrupole transition widths [ra01] proposed $b = 0$ as approximation. In the same paper $b = 0.36$ was applied in a more detailed comparison to calculations, performed assuming zero hexadecapole moments. Besides this ambiguity in b several definitions proposed as deformation parameters in the literature [hi53, ku72, bo75, ra01, de10] differ from the ‘standard’ definition as given here. Not all of them – even the ones in widespread use – conserve the volume when departing from spherical symmetry, especially for large β or Q_0 . This may lead to unwanted and often neglected contributions from compressional energy in respective calculations.

Intense experimental investigations [al56, ba73, ra01] concerning the energies and angular momenta of the levels in heavy nuclei have been regarded in view of single particle as well as collective excitations. In the data analysis and in theoretical studies [bo75] spherical or axial symmetry was usually assumed, albeit a sensitive experimental verification was missing. Here observed level energies and differences between them, eminent in gamma transition energies, have played an important role, in spite of eventual strong energy shifts due to configuration mixing. At variance the subsequent discussion focusses on electro-magnetic strength as indicator of nuclear collective motion, like rotation or vibration. An eventual breaking of axial symmetry may influence transition rates and it mainly results in new degrees of freedom which may enhance level densities and consequently radiative capture cross sections. Before respective predictions and observations will be discussed other indications for shape symmetry breaking in nuclei will be presented.

III. Quadrupole transition probabilities and triaxiality

The enhancement seen in experimental data on electric quadrupole (E2) transitions from the ground state [ra01] indicates a strong excess above predictions for a transition to a configuration formed by exciting only few particles. In connection to the observed quadrupole moments mentioned above this was linked [bo75] to the breaking of spherical symmetry in quasi all heavy nuclei away from magic shells. The model of a rotating axially symmetric liquid drop with a quadrupole moment, representing an even nucleus, predicts one 2^+ -state with a ‘collective’ *i.e.* enhanced E2-transition width. In this model the intrinsic structure for the ground state 0^+ and the lowest 2^+ -state r are assumed to be the same. Then the reduced matrix element (in $e \cdot \text{fm}^2$) of the electric quadrupole transition E_γ (in MeV) of this ‘rotational’ state r to ground is related [al56, bo75] to Q_0 (in fm^2) by:

$$|\langle r \parallel \mathbf{E2} \parallel 0 \rangle|^2 = B(\text{E2}, 0 \rightarrow r) = \frac{5}{16\pi} Q_0^2 \quad (2).$$

The E2 ground state decay width $\Gamma_{r0}(E_\gamma)$ (in MeV) is obtained from the general relation:

$$\Gamma_{r0}(E_\gamma; \text{E2}) = \frac{4\pi}{75} \frac{\alpha_e E_\gamma^5}{g(\hbar c)^4} |\langle r \parallel \mathbf{E2} \parallel 0 \rangle|^2; \quad g = \frac{2J_r + 1}{2J_0 + 1} \quad (3),$$

where α_e , \hbar and c are the fine structure constant, Planck’s constant and the velocity of light; J_0 and J_r are the spins of the ground state and the excited level. The reduced transition probability $B(\text{E2})$ used in (2) describes the rotation related quadrupole transition between the ground and the lowest 2^+ -state – it is often expressed in $e^2 \text{fm}^4$, but here – as in other papers – it is preferred to divide the E2 operator directly by the elementary charge e , and do this also with Q_s and $B(\text{E2})$. The latter are observables, whereas the deformation β is a model parameter, and in its relation to data one often assumes *ad hoc* a uniform axial charge distribution; the same assumption has been made [bo75] to relate axis ratios derived from IVGDR shapes to Q_0 or β . In view of ambiguities in the definition of β it will be used in the following in relation to theoretical calculations as defined there, whereas experimentally determined deviation from sphericity is expressed in units of an intrinsic quadrupole moment, whenever possible.

One serious shortcoming of the axial rigid rotor model is the fact, that it only predicts one ‘collective’ 2^+ -state. Experimentally at least two 2^+ -levels with enhanced transitions to the ground state are observed in nearly all even nuclei. This has led to the assumption [da65, bo75] that the coupling of the collective rotation to a collective quadrupolar vibration around an axially deformed basis state has to be invoked; it can either be along the symmetry axis (β -vibration) or perpendicular to it (γ -vibration) [bo75]. If for a respective Hamiltonian a solution is found, which describes the level scheme simultaneously to the $B(\text{E2})$ -values reasonably well one may consider this a determination of the mean values of β and γ , but for their dynamic uncertainty additional considerations are needed. Reference is often made to more microscopic calculations in a self-consistent scheme and various approximations [fo06, be07, ca09, li09, de10] have been proposed recently. The last of these calculations is available for practically all heavy even nuclei between the neutron and proton drip lines. In Fig. 1 the correlation between γ and Q_0 is depicted for nuclei in the valley of stability as it results from this CHFB-calculation. Assuming only \mathcal{R}_π -invariance they find non-zero triaxiality $\langle \gamma \rangle \neq 0$ for many nuclei, and in some cases the predicted standard deviation does not include $\gamma = 0$.

The CHFB calculations used here “*are free of parameters beyond those contained in the Gogny DIS interaction*” (adjusted to the properties of nuclei with small Q_0) and based on “*a density-dependent HFB approximation. They describe simultaneously the gross properties depending on the average field as well as the fine effects of the pairing correlations via the Bogolyubov field with the same force*” [de10]. The use of constrained wave functions allows to project on good angular momentum, which is important at low angular momentum.

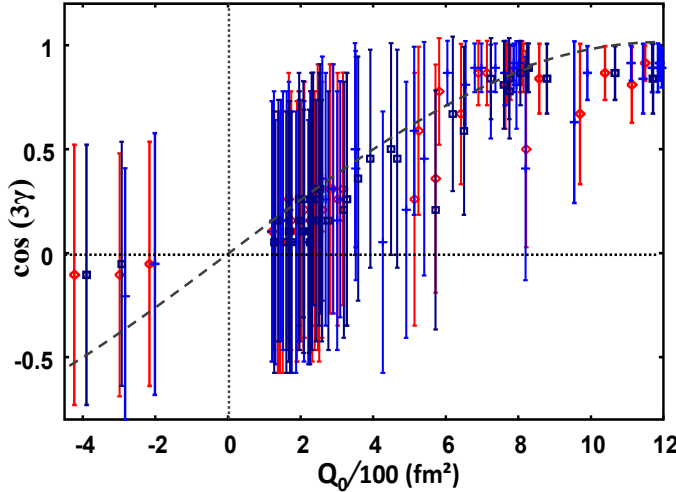


Fig. 1: Correlation between $\cos(3\gamma)$ and Q_0 in ≈ 170 even nuclei with $60 < A < 240$; the respective data are taken from a CHFB+GCM calculation [de10] for nuclei in the valley of stability. Red bars (\ominus) correspond to the minimum of the valley of stability, light blue (+) to nuclei with two less, and dark blue (\ominus) with two more neutrons. The bar lengths represent the standard deviations in γ as given by these calculations and tabulated as supplemental material.

Long ago it was pointed out [ha84], that information on triaxiality obtained for the intrinsic system in Hartree-Fock-Bogoliubov (HFB) calculations are subject to significant change when projected after variation into the observer’s frame: The γ -oscillation becomes centred at $\langle \gamma \rangle \neq 0$. A rather convincing agreement for E2-transition data is achieved by introducing a group theoretical ansatz to parameterize the quadrupole degrees of freedom as seen by the observer in the laboratory. Adjusting parameters for a given region of the nuclide chart by comparing to experiments this interacting boson approximation (IBA) [ar81, st84, jo07] is then used to predict transition probabilities as well as level energies for other nuclei in that region. A global description of all heavy nuclei was not reached yet, but by a distinction between neutron and proton modes an account for triaxiality was made (IBA-2) [ia03]. It should be pointed out, that such a ‘Bosonisation’ on the basis of data taken in the laboratory avoids problems related to the necessary projection into the observer’s frame, mentioned previously [ha84, fr01, de10]. Another way to circumvent these problems is the construction of rotation invariants from experimentally observed transition rates [ku72]. Data from of heavy ion induced multiple Coulomb excitation of low lying levels in heavy nuclei were analysed on the basis of rotation invariants [cl86, zi02] and for many heavy nuclei the breaking of axial symmetry was indicated by these experimental data. Such an analysis goes beyond an older, comparatively simple, model of a rigid triaxial rotor [df58] which directly delivers two collective 2^+ -levels. Generalizing Eq. (2) Q_0 is replaced by Q_i defined by the sum of several (in the case of a rigid triaxial rotor 2) squared E2-matrix elements:

$$Q_i^2 \equiv \frac{16\pi}{5} \sum_r |\langle r || \mathbf{E2} || 0 \rangle|^2 \quad (4).$$

Experimental data [pi94] show that a limitation to one term in the sum leads to an error of less than 10% in Q_i and thus for the figures an approximation could be done by using Eq.(3) instead of Eq.(5) to derive Q_0 from the calculated $B(E2)$ -values. In the rotation invariant ansatz [ku72] the deviation from axial symmetry is described by the parameter $\cos(3\gamma)$, which is directly related to the observable transition rates between the two 2^+ -levels r and s and the ground state 0 (in this model the sum is restricted to one term):

$$\cos(3\gamma) = -\left(\frac{16\pi}{5}\right)^{3/2} Q_i^{-3} \sqrt{\frac{7}{10}} \sum_{r,s} \langle 0 || \mathbf{E2} || r \rangle \langle r || \mathbf{E2} || s \rangle \langle s || \mathbf{E2} || 0 \rangle \quad (5).$$

As in quantal systems like nuclei only expectation values are accessible to measurements $\cos(3\gamma)$ and Q_i in Eqs.(3-5) are to be understood as such; in multiple Coulomb excitation the actually determined quantities are $\langle Q_i^2 \rangle$ and $\langle Q_i^3 \cos(3\gamma) \rangle$ requiring another approximation to derive the triaxiality [cl86, wu91, wu96, sr06, wr12]. In various nuclei the inclusion of triaxiality produced transition rates close to data [ma61, po73]. But, as in most heavy even nuclei more than 2 collective 2^+ -levels are observed, this scheme has to be generalized further. Employing tensor algebra and assuming reflection symmetry as well as identical distributions of protons and neutrons Eqs. (4) and (5) were shown [ku72, cl86, sr06] to be valid also for heavy nuclei in general, when they include all collective 2^+ -levels (to enter in the sum over r , s , *etc.*). As long as the sum includes all relevant 2^+ -levels Eq.(4) with $r > 2$ represents an un-weighted sum rule which is rotation invariant and thus valid in the laboratory as well as in the intrinsic frame. Assuming \mathcal{R}_π -invariance only Eq. (5) allows a relations for the three axes R_k of the ellipsoid to be derived in the body fixed system [ku72]:

$$5Q_i \cos(\gamma) = Z(2R_3^2 - R_1^2 - R_2^2); \quad 5Q_i \sin(\gamma) = \sqrt{3} Z (R_1^2 - R_2^2); \quad R_0^3 = R_1 R_2 R_3 \quad (6).$$

Invoking the concept of an equivalent ellipsoid, which has the same charge Ze , volume $V = 4/3\pi R_0^3$, and quadrupole moments as the nucleus, the three harmonic oscillator constants ω_k of the equivalent ellipsoid, are inversely proportional to R_k . With these equations they can be derived from the information about R_0 , Q_i and γ of a non-spherical nucleus, but not from the $B(E2, 0 \rightarrow r)$ alone. It should be pointed out here, that Eq. (3) of ref. [de10] relates the deformation values to the oscillator parameters, the direct outcome of these calculations. Thus the extraction of axis ratios differs formally from Eq. (6) as well as from the Hill-Wheeler formula used by us before [ju08]. It is straightforward to show numerically, that for the small Q_0 in the range of interest the differences are not significant. For the calculation of fission barrier heights more exact prescriptions may be needed, but, as was pointed out already [la73, gi82], the consideration of triaxiality is even more important in that case. In Fig.2 the correlation of the parameters Q_0 and $\cos(3\gamma)$ is displayed for more than 150 nuclei, for which relevant data have been published [cl86, st84, wu91, an93, wu96, es97, zi02, we05, sr06, wr12]. The rather complex experimental investigations on triaxiality were performed for a limited number of nuclei only, but a comparison to the prediction [de10] shown in Fig. 1 indicates a clear trend to triaxiality with decreasing Q_i is obvious ($\cos(3\gamma) \rightarrow 0$), whereas most well deformed nuclei show smaller deviation from axiality. The small number of nuclei which are oblate already at low E_x ($\cos(3\gamma) < 0$) does not allow similar conclusions, and for very small Q_i an analysis using Eqs.(5) and (6) is not appropriate.

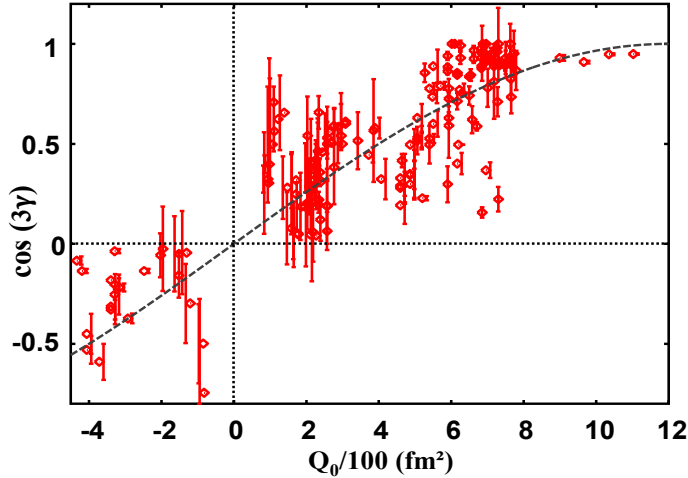


Fig. 2: Correlation between $\cos(3\gamma)$ and Q_0 in ≈ 150 even nuclei with $A > 60$, for which respective experimental data are available. The bars correspond to experimental uncertainties and the blue dashed curve serves as eye guide to compare the trend of the data to the one of the calculations as presented in Fig. 2, where it is depicted as well.

If not determined directly, the sign of the latter was assumed to coincide with the one of $\cos(3\gamma)$; different signs for these two quantities did appear only in few (≤ 4) questionable cases. These are omitted in the Figure as well as γ -values from data for odd nuclei [me74] which support the findings presented here. Also not given in the Figure are variances that can be derived in principle from an extension of the above formulae [ku72, cl86, sr06, wr12], but the experimental uncertainties of respective data do allow a rough extraction of such information only. The calculation shows a very similar trend of the axiality increasing with Q_0 as seen in the experimental data; at variance to Fig. 1 the density of symbols is now of significance, as all the nuclei from a small band near beta-stability were depicted. The trend as indicated as blue dashed curve in Figs. 1 and 2 suggests an approximation of nuclear shapes by only one parameter Q_0 , with axiality depending on it.

In the present review the γ -values are of interest mainly as indicator of broken axial symmetry and the influence of this feature on level density will be discussed below. The similarity between observation and the CHFB-calculations [de10] suggests their use in the theoretical shape parameters to evaluate the effect on the electromagnetic strength as derived from photonuclear data in the IVGDR region and below. The split of the dipole resonances relate to the three axis lengths $R_{x,y,z}$, and the equivalent sphere radius $R_0 = \sqrt{5/3} \langle R_p \rangle$ with the proton radius R_p also tabulated [de10]. The clustering at $Q_0 \approx 200$ fm 2 and $\cos(3\gamma) \approx 0.2$ seen in Fig. 2 is significant and will play an important role for the discussion of IVGDR shapes in the numerous transitional nuclei, often assigned an ‘intermediate’ shape.

IV. Photon absorption sum rules and giant resonances

The non-resonant interaction between photons and objects of charge Ze and mass M is quantified by the Thomson scattering cross section $8\pi(Z^2\alpha_e\hbar\cdot c)^2/3(Mc^2)^2$ with α_e denoting the fine structure constant, c the velocity of light and \hbar the Planck constant; for ^{208}Pb it amounts to 0.02 fm 2 only. A photon of sufficiently high energy $E_\gamma = E$ excites nuclei from ground also resonantly; this is described by a Lorentzian centred at E_r with total width Γ_r :

$$\sigma_\gamma(E) \cong I_{r0} \cdot \frac{2}{\pi} \frac{E^2 \Gamma_r}{(E_r^2 - E^2)^2 + E^2 \Gamma_r^2} \quad (7).$$

I_{r0} is the integral of the absorption cross section σ_γ over the resonance, which has spin J_r :

$$I_{r0} = \int \sigma_\gamma(E) dE = \frac{g (\pi \hbar c)^2 \Gamma_{r0}}{E_r^2}, \quad g = \frac{2J_r + 1}{2J_0 + 1} \quad (8).$$

The width Γ_{r0} is the partial width of the transition between the resonant level (E_r, J_r) and the nuclear ground state $(0, J_0)$. As described by Eq. (3) for $\lambda=2$, it is directly proportional to the electromagnetic transition matrix element; a respective relation exists for $\lambda=1$:

$$\Gamma_{r0}(E_\gamma; E1) = \frac{16 \pi}{9} \frac{\alpha_e E_\gamma^3}{g(\hbar c)^2} \cdot |\langle r || E1 || 0 \rangle|^2 \quad (9).$$

As derived from very general conditions like causality, analyticity and dispersion relations the interaction of short wavelength photons with nuclei of mass number $A = Z+N$ can be ‘integrated up to the meson threshold’ analytically, leading to the energy-weighted sum rule of Gell-Mann, Goldberger and Thirring (GGT) [ge54]:

$$I_{E1} = \int_0^{m_\pi c^2} \sigma(E_\gamma) dE_\gamma \cong 2\pi^2 \frac{\alpha_e \hbar^2}{m_N} \left[\frac{ZN}{A} + \frac{A}{10} \right] = 5.97 \left[\frac{ZN}{A} + \frac{A}{10} \right] \text{ MeV fm}^2 \quad (10).$$

Here m_N and m_π stand for the mass of nucleon and pion, respectively. The first term in the sum is the “classical sum rule” for electric dipole radiation (TRK, ku25) and the second “contains all of the mesonic effects” and is assumed [we73] to be accurate within 30%. It was approximated by assuming “that a photon of extremely large energy interacts with the nucleus as a system of free nucleons”, and a correlation to hadronic shadowing was investigated to be weak [we73]. Eq. (10) includes all multipole modes of photon absorption and no arguments [le50] about the nuclear absorption of photons with energies above $m_\pi c^2$ are needed. Absorption by the nucleons does not contribute below $E_\gamma = m_\pi c^2$, but nucleon pairs and especially p-n-pairs are strongly dissociated by photons with $20 < E_\gamma < 200$ MeV. The respective “quasi-deuteron effect” has been derived from the expression valid for the free deuteron by correcting for Pauli blocking [be50, ch91].

Photo-neutron data are available [Ah85] for ^{208}Pb up to energies above $m_\pi c^2$; they are shown in Fig.3 and compared on an absolute scale to respective theoretical expressions: (1) a Lorentzian like in Eq. (7) of width $\Gamma_r = 3.26$ MeV and pole energy $E_r = 13.6$ MeV, with I_r normalized such that its integral agrees to the first term in Eq. (10), and (2) the expression for the absorption corresponding to the quasi-deuteron mode [ch91].

Apparently the cross section above 40 MeV is well reproduced on absolute scale and it should be mentioned that its integral is close to the second term in Eq. (10). It is worth mentioning that a similarly agreement was published [ch91] for other nuclei. The enhancement between 20 and 30 MeV observed to exceed the sum of the two curves may be identified with the contributions from $T_{<}$ -component of the IVGDR [vc84] and the IVGQR [pi74, do82].

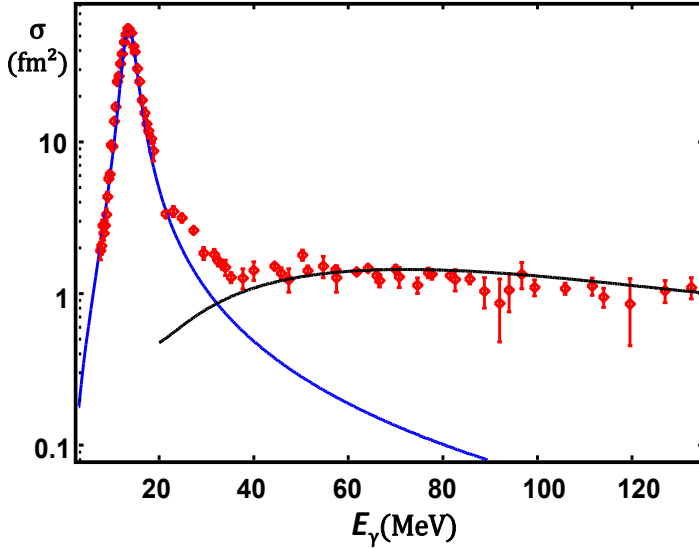


Fig. 3: Cross section of photo-neutron production data [Ah85] on ^{208}Pb in comparison to a Lorentzian for the isovector IVGDR (light line, blue) and the quasi-deuteron effect (heavy black line).

In contrast to elastic electron scattering [pi74, do82] the cross section shown in Fig. 3 shows only weak signs of giant resonances of multipolarity other than E1: M1:GMR, E2:GQR or higher λ . For the quadrupole giant resonances the energies are known in several nuclei from experiment with electron [pi74, do82] or hadron beams [ul87, yo04] such that the respective sum rule [na65] can be used to determine an upper limit of 5 % in Eq. (10). In a recent paper on the M1-strength in heavy nuclei measurements for many nuclei are reviewed [he10] and from the quoted values for M1-strength the contribution of that mode to Eq. (10) can be seen to be less than 3 %.

The photo-disintegration of nuclei is one of the first nuclear reactions studied; soon after it has been recognized as dominating photon absorption by an excitation of the IVGDR. This isovector nuclear electric dipole resonance represents a strongly collective oscillation of neutrons against protons. The two first theoretical descriptions describing this nuclear mode work rather well for medium mass nuclei [go48] as well as the very heavy ones [st50]. By using concepts of the droplet model these two approaches were unified [my77] and hence IVGDR centroid energies $E_0(Z,A)$ are well predicted in the range $50 < A < 254$. The good agreement in the region below 20 MeV seen in Fig. 3 indicates that the first term in Eq. (10), a Lorentzian in accordance to the classical electric dipole sum rule (TRK, [ku25]) is a good ansatz to describe the IVGDR. Although it is not a distinct quantum level, but a sum of densely packed levels resonantly enhanced near the ‘pole energy’ $E_r=E_0$, it is described well. Derived from Eq. (7), but now applied to a wide giant ‘doorway’ forming an envelope over narrow electric dipole states excited by E1 radiation, Eq. (11) is used for the parameterisation of the IVGDR. The possibility of a Lorentzian was predicted theoretically [do72] and tested numerically at hand of data for a few nuclei [go77]. To normalize the sum of k Lorentzians, with k characterizing an eventual split, the main term of Eq. (10), the classical sum rule, is divided equally into k portions:

$$\frac{dI_{\text{E1}}}{dE_\gamma}(E_\gamma) \equiv \sigma_{\text{abs}}^{\text{E1,IV}}(E_\gamma) \cong 5.97 \frac{ZN}{A} \frac{2}{k\pi} \sum_k \frac{E_\gamma^2 \Gamma_k}{(E_k^2 - E_\gamma^2)^2 + E_\gamma^2 \Gamma_k^2} \text{ fm}^2 \quad (11).$$

It will be shown in the next section, that the TRK sum rule is especially well fulfilled, when the breaking of axial symmetry is taken into account. The different axis lengths as introduced by Eq. (6) relate to the splitting of the IVGDR, especially obvious in the experimental data [be75, di88] for the lanthanide and actinide nuclei. It will be discussed in section V how good an agreement to strength data is obtained not only for the region of the maximum, but also in the low energy tail. In Fig. 3, here approximating ^{208}Pb as spherical even above 10 MeV, $k=1$ is used. For heavy nuclei only very few parameters for pole positions and resonance widths are required in a global fit: The droplet model predicts the IVGDR centroid energies $E_0(Z,A)$ [my77] in the range $50 < A < 250$. The nuclear radius used here is derived from the mean charge radius $\langle R_p \rangle$ taken from the CHFB calculations [de10] as $R_0 = \sqrt{5/3} \cdot \langle R_p \rangle$; symmetry energy $J=32.7$ MeV and surface stiffness $Q=29.2$ MeV are taken from the finite range droplet model [mo06]. Only one additional parameter, an effective nucleon mass has to be adjusted [ju08] to $m_{\text{eff}} = 800$ MeV/c² in an overall fit to the IVGDR data and the E_k are derived from the E_0 in accordance to the CHFB calculations (cf. Eq. (6)).

The nature of the IVGDR forbids the determination of its width in analogy to Eq. 9, and the widening due to deformation has to be accounted for by using $k > 1$ in Eq. (11). A strict distinction between damping or spreading and the deformation induced splitting – to be discussed below – results in a photon energy independence of the widths extracted from IVGDR data. Hydro-dynamical considerations [bu91] predict the dependence of the damping width Γ_k of an IVGDR on its pole energy E_k to be proportional to $E_k^{1.6}$; this exponent lies between theoretical values [fi85] for one- and two-body dissipation. With one parameter adjusted to be equal for all heavy nuclei with $A > 50$ one gets in good agreement to experimental findings [en92, ju08] - if both in are expressed in MeV:

$$\Gamma_k = c_w \cdot E_k^{1.6} \quad (12).$$

Of course, the proportionality constant c_w has an uncertainty related to the selection of nuclei, which are included in the fit. With the axis ratios available from the CHFB calculations an inclusion of all nuclides for which respective data have been tabulated [ex14] yields $c_w = 0.045(3)$. It is stressed here, that the width parameter is varying with E_k and not with E_γ in agreement to data [ju08]. As the slope of a Lorentzian sufficiently far away from E_0 is quasi proportional to Γ_k ; its uncertainty enters in the radiative width nearly linearly. Recently, a value of $c_w = 0.05$ had been found [ju10] when single Lorentzians were adjusted to IVGDR data for ^{88}Sr and ^{208}Pb , assumed to have one pole only. The new value given here is based on the calculations [be07, de10] and also accounts for the influence of the GQR's, as will be regarded below.

Individual local fits [di88, pl11] to the apparent widths seen in photo-neutron data (using $k=1$ or 2 in Eq. 11, selected *ad hoc* to optimize the fit) result in a surprisingly large excess above the TRK sum rule. The fit [pl11] depicted in the top part of Fig. 4 differs some from earlier data analyses [be75] which yielded an average of 105 (8) % for $100 < A < 200$ and a finding for six Sn-isotopes, where an overshoot of only 10(7) % was found [fu69]. The large unsystematic scatter reported from both local fits yield strong arguments against their use for nuclear astrophysics, albeit proposed [gy98] in that field.

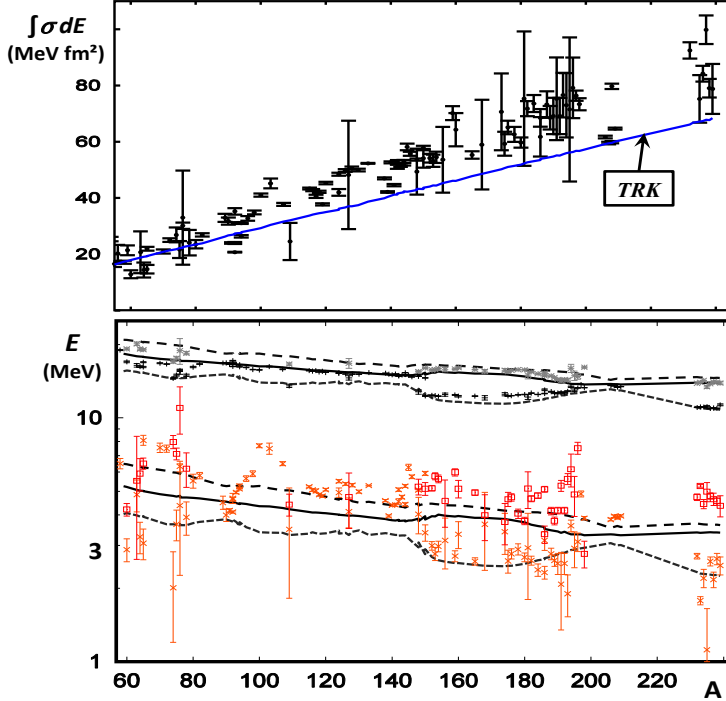


Fig. 4: The lower plot shows the energies (top) and widths (bottom) of the IVGDR in heavy nuclei vs. mass number, as resulting from χ^2 -fits compiled recently [pl11]. The fits are based on one or two Lorentzians and two points per nucleus are shown, if a 2-pole fit led to a smaller χ^2 . Calculations as described in section V (TLO) are depicted as drawn curves. In the upper plot the resulting GDR-integrals as obtained from the Lorentzian fits are depicted in comparison to the TRK sum rule, which is surpassed considerably in most cases. Data are from ref. [ca09].

The lower panel of Fig. 4 shows how the pole energies and Lorentz widths from the local fits as published recently [ca09, pl11] scatter as compared to the description of the IVGDR shapes, allowing three poles and thus a ‘triple’ Lorentzian (TLO) parameterization. This is a preview to the predictions derived from the global fit procedure detailed in the next section. As seen from Fig. 4 the TLO-method results in a smooth dependence on A which is modulated only due to variations in shape. And the comparison to various photon data in IVGDR peaks and their tails as presented in sections V to VII shows that the new ansatz clearly agrees better with data than shown by previous works [be75, di88, pl11]. But care is indicated with respect to a detailed comparison within narrow energy bins: For some nuclei near magic shells the level-density is rather small up to the IVGDR peak (and far below a Fermi-gas prediction; cf. section IX) such that fluctuations are observed as long as the experimental averaging is comparatively small.

Obviously, several components may be responsible for the apparent width of the IVGDR in heavy nuclei:

- (a) Spreading into underlying complex configurations,
- (b) Nuclear shape induced splitting,
- (c) Fragmentation and
- (d) Particle escape.

From calculations for heavy nuclei using the Rossendorf continuum shell model [ba77, be11] the escape widths (d) in the IVGDR region were shown to be clearly smaller than the effect caused by damping or spreading as predicted by eq. (12). For the concept of fragmentation

(c) of the configurations belonging to e.g. the IVGDR a calculation of these configurations is needed. Regarding the detailed shell model calculations [sc10, br00] for the nucleus ^{208}Pb depicted in Fig. 5, which is based on a large number of configurations, one comes to the conclusion that the parameterization of this IVGDR by a Lorentzian with no width-dependence on photon energy finds additional support.

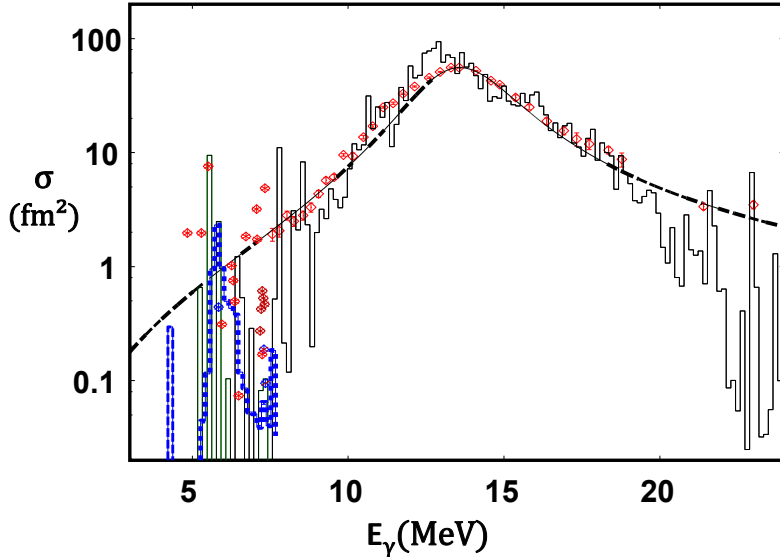


Fig. 5: Dipole absorption from a shell model calculation for ^{208}Pb with configuration mixing [sc10; black: $E1$, blue dots: $M1$]. For comparison experimental data from photon scattering [sc10, \blacksquare] and absorption [ah85, \blacksquare] as well as the Lorentzian from Fig. 3 are superimposed.

Such a decrease was postulated by the KMF-model prediction for f_{E1} allegedly derived from the theory for Fermi liquids [ka83]. A detailed relation to the work of Landau or Migdal is not given in that work, which explicitly states below Eq.(29), that a *direct comparison* between the *spreading width* in a Lorentzian for the GDR and the one of the *theory of Fermi liquids* is *difficult...and not clear* [ka83], and they further *assume* ad hoc without any additional arguments, that they *coincide*. In this context it should be mentioned that fundamental theoretical arguments have been used to show, that “*Landau damping is not the appropriate process for describing the damping of the low-multipole giant resonances*” [fi85].

V. Isovector giant dipole resonances in heavy nuclei and triaxiality

Since long time, the coupling of dipole and quadrupole degrees of freedom in heavy nuclei has been discussed [da58, da64, da65, bo75, na91] and calculations within the interacting Boson model (IBA) have obtained reasonable fits to experimental data for two chains of even isotopes [ma84] and some other nuclei [ho91, zh09]. In the dynamic collective model (DCM) [da64, se74] calculations on the basis of hydro-dynamical considerations were successfully compared to selected data [bo81, bo83]. The importance of the breaking of axial symmetry for the GDR shapes was not discussed in the literature cited here and not in most of related work. In theoretical papers on a few nuclei triaxiality was mentioned with respect to the IVGDR [bo90, bu91], but a full coverage of a wide range in the nuclide chart is missing. The parameterization presented earlier [ju08] and specified in this section is much less ambiguous concerning the mode coupling, but it has one advantage as it incorporates nuclear triaxiality explicitly by setting $k=3$ in Eq. 11. For the resulting ‘triple’ Lorentzian (TLO) description the

resonance energy E_0 is modulated by the ratios of the axis lengths R_k in the spirit of Eq. (6) by setting $E_k/E_0 = R_0/R_k$. This direct incorporation of triaxiality makes TLO differ from previous attempts to obtain Lorentzian fits to photo-neutron data for a large number of heavy nuclei [ba73, be75, bo75, di88, ko90, ca09, pl11]. In many nuclei, especially those of intermediate Q_0 , the local fits presented there may lead to a seemingly better agreement, but often they require quite unreasonably large values for the damping width of the IVGDR and for the integrated strength in comparison to sum rule predictions. If triaxiality is accounted for in addition to the quadrupole deformation a good description of IVGDR shapes is obtained without treating the strength and width as free fit parameters. The deformation induced shift of the three axis lengths R_k versus the equivalent radius R_0 is obtained from Eq. 3 of the CHFB calculation [be07, de10]. As outlined in section III, this work lists values for the quadrupole deformation β as well as the corresponding γ for a large number of even nuclei. Hence, a global prescription to predict electric dipole strength can be derived from it, not limited to using local information for single nuclei.

When a parameterization of the electric dipole strength in non-spherical nuclei is aimed for, the contribution (b) of the list in the previous section has to be treated sufficiently well. As shown in the top part of Fig. 4, the TRK sum rule, Eq. (10), disagrees in many nuclei to the Lorentzian fits [di88, pl11] performed for the data of each nucleus independently without account for the possibility of broken axial symmetry. In these fits the width parameter was adjusted for each isotope separately to fit the peak region and for A between 90 and 150 an especially large discrepancy is observed as well as wide fluctuation with Z and A of this apparent width indicating a non-systematic variation which is difficult to conceive within the spreading concept. A similarly erratic dependence of the integrated IVGDR strength on Z and A was reported [pl11] to result from this approach of fitting the photo-absorption data locally. In some cases the integrated cross section overshoots the classical sum rule given by Eq. (10, first summand) by up to 100%. Apparently the two problems named are closely related, as the resonance integral is proportional to the product of height and width. As proposed previously [ju08, na10, er10], a solution for this problem is found by allowing axial symmetry to be broken; this point will now be examined in further detail. As shown in section III accurate nuclear spectroscopic data suited to determine both deformation parameters are available only for a limited number of nuclei. The recent CHFB calculation [de10] discussed there and depicted in Fig. 1 reproduce quite well the trend of experimental deformation data vs. A shown in Fig. 2. With this paper [de10] supplemental material is given for 1712 even-even nuclei including their deformation and from Eq. (3) in it the corresponding ‘*triaxial oscillator parameters*’ can be derived, similar to the axis lengths from Eq. (6) above. This prior information is inserted to obtain the resonance energies in the sum of Lorentzian functions in Eq. (11) to be compared to experimental data for the IVGDR. This procedure leads to a splitting into three equally strong IVGDR components which increases with β and γ taken from the calculations [de10]. As seen in Fig. 4, for many nuclei the splitting between the three components is comparable in energy to their widths and thus not suggested strongly from the data alone, especially in nuclides with $Q_0 \approx 200\text{-}300 \text{ fm}^2$. These are not rare as the clustering depicted in Fig. 2 shows, but the knowledge about triaxial deformation demands that all three axes are accounted for explicitly. This quite simple consideration explains the significant rise in apparent width as seen in Fig. 6 for the even Sm-isotopes with $N=86$ to $N=92$; ^{144}Sm was

not included because of the unknown cross section for the (γ, p) -reaction.

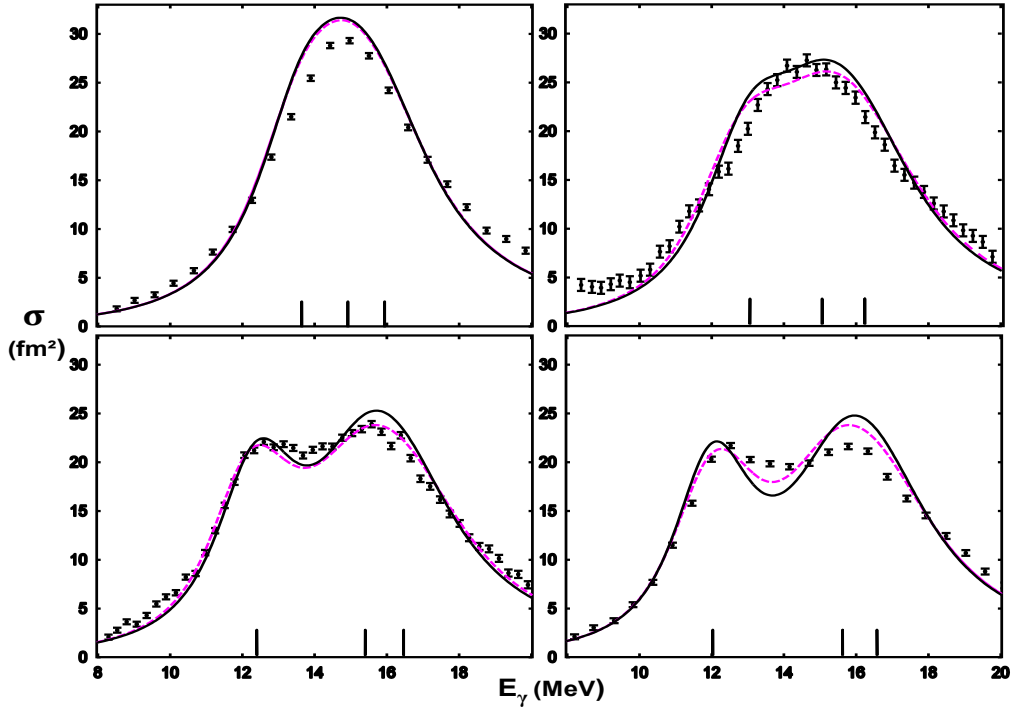


Fig. 6: Cross section [ca74] of photo-neutron production on ^{148}Sm (top left) to ^{154}Sm in comparison to the TLO sum of three Lorentzians (drawn curve) with E_k indicated as black bars. The dashed (purple) curves indicate the effect of shape sampling [zh09, er10, gr11]. As outlined in the next section the data were renormalized by a factor 0.9 and the calculations were folded with a Gaussian to simulate an experimental beam spread of $\sigma \approx 0.2 \text{ MeV}$ [au70].

Fig. 6 shows results for the Sm-chain; in slightly deformed nuclei as ^{148}Sm , previously often regarded as spherical, the deformation induced split in combination to the small width parameter in Eq. (12) leads to a low tail, which is of importance for the envisaged extrapolation to even smaller energies. Special care is needed for nuclei near closed shells: The CHFB calculations do not fully account for the very deep mean field potential in such nuclei and thus they produce too much of collectivity [be07]. Following what is said there, a reduction for nuclei only δ nucleons away from a shell a factor for the β -deformation of $0.4 + \delta/20$ is applied for $\delta \leq 12$. This expression results in a reduction of the predicted [de10] β -values of 40, 30, 20 and 10 % for the isotopes ^{148}Sm , ^{150}Sm , ^{152}Sm and ^{154}Sm ; the corresponding agreement to the IVGDR data is shown in of Fig. 6. It is worth mentioning here, that the increase of width with E_k as predicted from Eq. 12 reduces the maximum in the upper of the two peaks, such that it is not two times higher than the lower, as expected from the prolate near axiality of ^{154}Sm .

The supplemental material based on the CHFB-calculations [de10] does not only list the mean values for the deformation parameters as obtained via the GCM, it also gives their variances as resulting from quantum mechanical zero point oscillation effects. The respective Gaussian distributions obtained thus allow an instantaneous shape sampling (ISS) as shown earlier [zh09] for isotope chains Mo [er10] and Nd [gr11]. There the impact of ISS on the height of the low energy tail and thus on radiative capture was shown to be negligible. Results for the Sm chain as shown in Fig. 6 have a minor influence as well: the drawn black curves

correspond to the TLO-prediction and the dashed purple curves stem from the analysis with TLO + ISS. The investigation of this effect for other nuclei needs further study. The self-consistent extension to non-spherical nuclei introduces no extra free parameters in addition to the global ones of the Gogny-force [de10] and an attempt of a fit to the IVGDR energies and widths succeeds with only the four parameters introduced in connection to Eqs. (11 and 12), two of which are known from LDM mass fits. In the evaluations presented in the next section the only local parameters for individual nuclei are the axis ratios calculated by CHFB [de10], and no dependence of the widths Γ_k (cf. Eq. 12) on the photon energy E_γ was allowed – at variance to a proposal made [ko90] on the basis of the KMF model [ka83]. Invoking widths varying only with the pole energies E_k (and not with A and Z) opens the possibility for a global prediction of nuclear photon strength also for heavy exotic nuclei and the extension to energies below the neutron emission threshold S_n is of interest. This may open a potential of consistent predictions for radiative capture processes, where full satisfaction is not reached with presently available methods [be14]. But, as will also be discussed below, other modes than the IVGDR contribute to photon absorption and their influence will be quantified in sections VIII and X.

VI. Electric dipole strength in the IVGDR and below

The interaction of photons with heavy nuclei at energies above the neutron separation energy S_n is mostly resulting in reactions of type (γ, xn) , but for a determination of the complete absorption cross section the emission of p, α 's or fission might also be important. As will become obvious (and indicated already in Fig. 5) the photon absorption in nuclei with low level density below the IVGDR pole may be fragmented into many small peaks, which become unresolved and finally overlapping at higher excitation energy. The radiative neutron capture discussed later is partly influenced by unresolved resonances and it is thus indicated to use average photon strengths f_λ for the description of their electromagnetic decay by multipolarity λ . This average quantity, the strength function $f_\lambda(E_\gamma)$, was introduced [ba73] for electromagnetic transitions. Their relation to the average photon absorption cross section and the integral I_{abs}^λ over a given energy interval Δ_E around E_γ is:

$$f_\lambda(E_\gamma) = \frac{\langle \sigma_{abs}^\lambda(E_\gamma) \rangle}{(\pi \hbar c)^2 g_{eff} \cdot E_\gamma^{2\lambda-1}} = \frac{I_{abs}^\lambda}{(\pi \hbar c)^2 g_{eff} E_\gamma^{2\lambda-1} \Delta_E} \quad (13)$$

To use the strength functions $f_\lambda(E_\gamma)$ for excitation as well as decay processes (Axel-Brink hypothesis) and thus connect photon scattering to radiative capture and photonuclear processes one has to suppose them to be direction independent [ba73]. Eqs. (8, 9 and 13) may then be used to directly relate f_λ to the electromagnetic decay widths of the resonant levels r in the integration interval Δ_E and the reduced matrix elements for their transition to ground:

$$f_\lambda(E_\gamma) = \frac{1}{\Delta_E} \sum \frac{\Gamma_{r\gamma}}{E_\gamma^{2\lambda+1}} \cong \frac{\langle \Gamma_{r\gamma}(E_\gamma) \rangle}{D_r \cdot \bar{E}_\gamma^{2\lambda+1}} \quad (14).$$

The integration in Eq. (13) runs from $E_\gamma - \frac{\Delta E}{2}$ to $E_\gamma + \frac{\Delta E}{2}$ and for the sum in Eq. (14) all levels within this interval are included; the quantum-mechanical weight factor g_{eff} will be discussed

in section VII. The average level spacing D_r at the upper of the two levels connected by $E_\gamma = E_r - E_f$ is related to the level density $\rho_r = 1/D_r$. Increasing $\langle \Gamma_r(E_\gamma) \rangle$ results in an increase of $f_\lambda(E_\gamma)$, but branching decays have to be corrected for [ax70], and thus ρ_f also plays a role when applying Eq. (14) to data. Such decays may take place between levels which are both excited and there is no direct way to study them starting from target ground states. But the average quantity f_λ is assumed to be insensitive to details of the nuclear excitations and one thus approximates collective electromagnetic transition strengths of energy E_γ by $f_\lambda(E_\gamma)$ to be independent of the energies E_r and E_f ; together with the notion of f_λ being valid for excitation and decay, this assumption is called Axel-Brink hypothesis [br57, ax62]. In the present ansatz an eventual dependence of decay strength on a temperature near the final state is accounted for by averaging over that region using a level density which may deliver an apparent temperature (cf. section IX).

Several facts have to be regarded when using experimental photo-neutron or photon absorption data to test the TLO parameterization as strength-function prediction:

1. Considerable discrepancies were reported for experiments performed e.g. at different laboratories [be87, ut08, ut11]; in some cases energy calibrations may differ somewhat.
2. Photo-neutron data were often obtained by using quasi-monochromatic photon beams with a rather wide energy distribution, which is incorporated by folding the calculations with a Gaussian of width $\sigma = 0.8$ MeV [va04, va14], an increase to optimize near the peak, as will be depicted in Figs. 15 and 25. If a bremsstrahlung distribution is used for such studies a complex subtraction method is needed inducing some uncertainty [fi83].
3. In a number of cases the (γ, p) -channel exhausts a significant portion of the photo-absorption cross section [di88, er10, pl11]. It was shown in an earlier paper [er10], how the eventual influence of all open channels on the extraction of the absorption cross section from the existing data is tested by Hauser-Feshbach calculations.
4. At higher energy the competition by the $(\gamma, 2n)$ channel becomes important and that requires involved subtraction procedures [bo83], which may be questioned [va04, va14].
5. Most of the targets used contain unwanted isotopes, and when some of them have a lower S_n (like many odd isotones) the low energy yield has to be corrected.
6. Below and above the pole of the IVGDR contributions from the giant quadrupole (GQR) modes cause effects of some significance.
7. In heavy nuclei various excited states may exist aside from giant resonances, which cause observable photon strength also below the neutron threshold. It adds to the IVGDR tail not always smoothly, as Porter-Thomas fluctuations [ax62] may create strong peaks in spectra statistically from a quasi-continuum of weakly populated levels.

In the IVGDR region averaged experimental photo-dissociation data as obtained with quasi-monochromatic photons from positron annihilation have been compiled and are available [be75, di88, ex14]. Such data do not exist for all stable isotopes and for some nuclei photo-absorption has been studied by an extinction technique, which may serve for a consistency check in spite of its systematic error due to the need to subtract the strong atomic absorption. As indicated repeatedly [ca71, be71, be87, is04, va12, sa14], cross sections obtained at Saclay should be reduced. In accordance to a precision study [be87], confirmed by results [na08,

er10] from the radiation source ELBE, the photo-neutron data of the Saclay group are hence multiplied in this work by 0.9, as suitable mean over A. Items 2 to 4 influence the representation of the IVGDR peak region, but their effect on the tail a few widths Γ below the pole is insignificant – in contrast to points 5 and 7.

Photon strength data for energies below S_n are even rarer [ju08]. Similar as in many photo-neutron studies experiments with quasi-monochromatic beams are performed to gain information on absorption from photon scattering: In early experiments the tagging system at Urbana was used [ax70, la79] and an increasing number of measurements are done at the laser-photon backscattering facilities HI γ S (High Intensity γ -Ray Source) at Duke University [we80, to10] and AIST (National Institute of Advanced Industrial Science and Technology) in Japan [ut11]. The photon intensities from these are not well known and bremsstrahlung data may serve for normalization. Results from scattering have to be corrected for branching to other than the ground state and in various cases the bremsstrahlung continua also feed higher excited levels and their decay yield has to be subtracted. In the case of less complex spectra use can be made of data from the decay to well isolated levels [ju95, go98]. More sophisticated schemes as developed *e.g.* at ELBE [ru08, sc07, sc10, er10, sc11] are based on statistical considerations already formulated previously [ba73, ax70]. Due to the fact, that the electromagnetic strength is responsible for the absorption as well as the emission of photons, an iterative procedure can lead to a self-consistent solution [sc11, ma12, ma14]. Here, level spacings enter which often were taken from predictions and extrapolations eventually questioned; in view of new results [gr14] on level densities as outlined in section VIII a reduction of 30% in the f_λ as compared to published data was applied in three cases. All the data covering the region below S_n and hence the IVGDR complement the information from photo-neutron studies. Here also photons observed after nuclear collisions can deliver strength-information, when their yield can be normalized via an ‘external’ fix-point. In the case of resonant neutron capture this is realized by ‘*using the absolute gamma-ray intensities due to captured thermal and resonance neutrons*’ [mu00]. A similar normalization via neutron capture, now with respect to level densities, was attempted for data taken at the Oslo cyclotron [vo04, gu05, si06] with ^3He and d projectiles. The method of relying on neutron capture resonance spacings requires the knowledge of the energy dependence of level distances; here theoretical assumptions have been used like a constant temperature ansatz (CT) [gi65] or the Fermi gas (FG) model [er60], which until recently entered in the data analysis of the Oslo group. A reconsideration now favours the CT approximation [gu15, mo15] and thus it seems appropriate, to not fully rely on older strength function data from that group.

The subsequent compilation presents in Figs. 7 to 25 photon strength function data and a comparison to the TLO parameterization with three IVGDR pole energies induced by the deformation. Here parameters are taken from the available CHFB-calculations [de10] and globally determined fit values for c_w in Eq. (12) and an effective mass quantifying [ju08] the centroid E_0 . The (black) dashed lines represent the prediction of f_{E1} thus derived with the resonance integral from Eq. (11) (in accordance to the TRK sum rule) equally divided among the three. In all subsequent figures the three poles of TLO are indicated as black bars at the energy axis. Although the apparent peak-height depends on the split, the absolute heights in

the low energy slope are nearly unchanged. As shown previously [sc11] and as will be further detailed in section X, the effect of the photon strength on radiative neutron capture is strongest in the tail region. Thus ‘minor’ strength components below the IVGDR may be of importance; they will be detailed in section VIII, and – quasi in a preview – they are depicted by the full blue line in the subsequent figures. In the region above S_n E2-strength from the GDR is included in the plots after an adjustment that visualizes its influence on the photo-absorption cross section; E2-strength below S_n is not depicted, as only local information for it is available (for measured data via RIPL-3 [ca09], for calculations in ref.[de10], *e.g.*). No locally fitted quantities enter the calculations for the plots. These start at 2 MeV as below Thomson scattering by the nuclear charge surmounts the IVGDR tail and the zero at $E_\gamma = 0$ in Eq. (11); in γ -decay other processes [sc13] may become important as well. It should be stressed here again, that the presented ansatz does not result in a full theoretical understanding of the coupling between the IVGDR to quadrupole modes or of other excitations, but in a more phenomenological prediction of photon strengths, which is global and hence extendable to many nuclides. The nuclei discussed in the following compilation were selected such that photo-neutron data and results for energies below S_n are available; still different A , Z and Q_0 are well represented. Most data were taken from an electronically accessible data base [ex14], for which they had been extracted from original work; to improve the visibility of the data points, some of the excitation functions have been re-binned to around 0.6 MeV/bin. To arrive at better understandable figures, data were compressed eventually, and points of no significance were suppressed, *e.g.* when their uncertainty is comparable to the value. The nuclei regarded here will demonstrate what features of photon strength information can be derived experimentally. For nuclides as light as than ^{54}Fe channels competing to (γ, n) cause difficulties for the extraction of the absorption cross section and hence the photon strength. In view of an increase of this problem with falling A reasons for not extending the study to lower A are indicated.

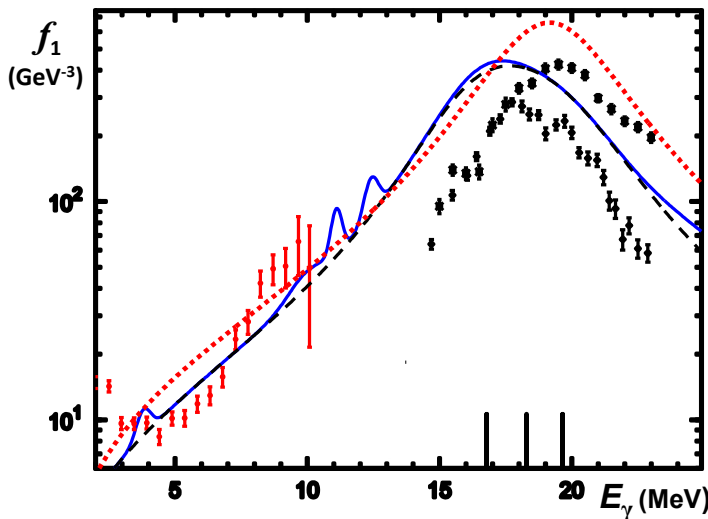


Fig. 7: Photon strength for ^{54}Fe predicted by TLO (dashed line). Data [no78] (Φ : γ, p ; and \blacksquare : γ, n) nearly coincide between 15 and 18 MeV, whereas at higher energy the (γ, p) channel dominates and their sum is rather close to the dashed line in black – on absolute scale. Photon strength data at low E_γ (\bullet) are for ^{56}Fe as obtained from γ -decay after He-induced processes [al08]. The influence of minor strength is depicted as full line in blue and the dotted line in red results from a one pole fit to the photon absorption cross section derived from these data [pl11].

Photo-dissociation data for ^{54}Fe [no78] are shown in Fig. 7 to be not far from the TLO prediction in the IVGDR, when the (γ, p) and (γ, n) channels are added up. The f_γ derived [al08] at lower E_γ from γ – decay in ^{56}Fe seem to agree reasonably well to the sum of TLO and considerable extra ‘pigmy’ strength near 7 – 8 MeV (cf. Table I). But it should be mentioned, that between 6 and 10 MeV two published data sets lie clearly below [ch84] and above [vo04], and this is a typical example for problems arising for the kind of survey study as presented here. The observed strong rise below 3 MeV does not correspond to any prediction considered in the present study, but it may eventually be similar to M1 strength recently predicted for some heavier nuclei [sc13]. For 11–13 MeV, where the spin-flip M1 strength is expected, no data are available.

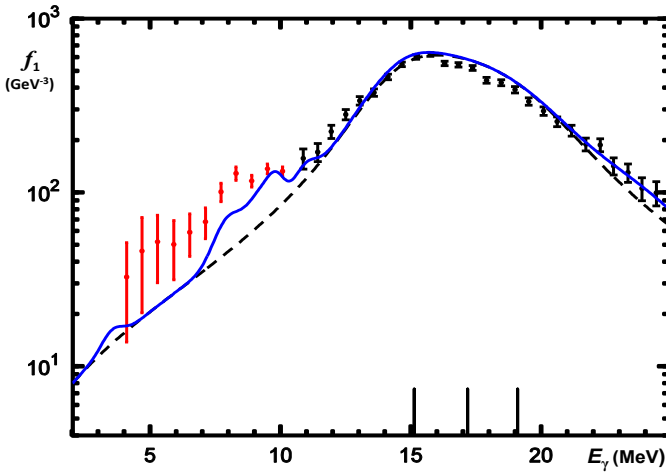


Fig. 8: Photon strength function for ^{78}Se (+[go82], \square [ca76]) in comparison to the TLO-prediction (dashed black line); an inclusion of minor strength is shown as full blue line. Photon scattering data at low E_γ (■) are obtained with bremsstrahlung from ELBE [ma13] reduced by 30 % in view of a ‘new’ level density ansatz, cf. section VIII).

In ^{78}Se a significant increase over the extrapolated tail is observed for $7 < E_\gamma < 10$ MeV, although the photon scattering data [sc10] were reduced by 0.7 to correct for the disagreement of the level density ansatz used in the data analysis [sc10] with the one published recently [gr14], which will be discussed in section IX. They were derived from photo-neutron experiments performed at Saclay [le71, be74] and from photon scattering investigated at the radiation source ELBE [sc05, ru08].

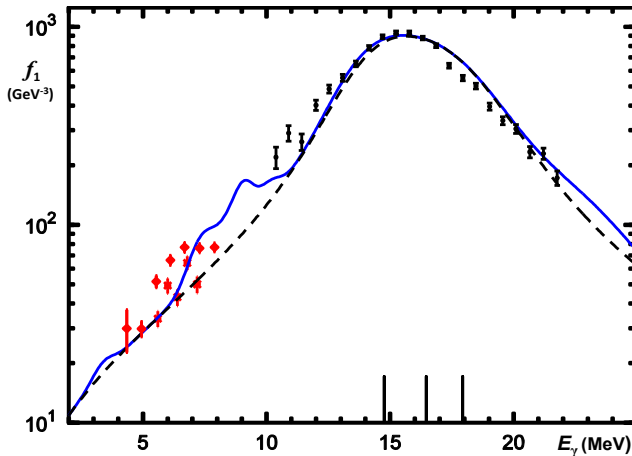


Fig. 9: Photon strength for ^{98}Mo from photo-neutron data [black open square: be74] in comparison to the sum of three Lorentzians (TLO). The data below 9 MeV are from elastic photon scattering $^{98}\text{Mo}(\gamma, \gamma)$ observed with bremsstrahlung [red open diamond: ru08] or monochromatic photons [red cross: ru09].

Photon strength functions have been published previously for ^{88}Sr [ju08, gr14], as well as for $^{92-100}\text{Mo}$ [er10]; a width independent of E_γ was used, a good agreement to the TLO prediction is observed and the integrated cross section obeys the TRK sum rule. The similarity between the low energy slopes in all Mo's led to the suggestion [ju08, er10] of an extrapolation with energy independent width and the assumption of broken axial symmetry allows the use of resonance widths which do no longer need a specific widening for each isotope. Looking at ^{98}Mo is of importance also for the detailed characterization of minor components, as this extra strength with impact on the tail below 10 MeV may contribute to radiative capture. Bremsstrahlung data corrected statistically for inelastic scattering [ru08, er10] are very close to newer results obtained with quasi-monochromatic photons [ru09].

At variance to this agreement photon strength function derived from inelastic ^3He scattering [gu05] are nearly a factor of 3 smaller at 7 MeV as compared to the data as shown in Fig. 9, and this may indicate, that the so-called Oslo method may suffer from the normalization to photon strength observed by neutron capture. The recently revised data [la10, ut11] agree around 7 MeV to the photon scattering results and thus also to the TLO prediction with minor strength added. These new data overshoot at higher E_γ and are lower by $\approx 40\%$ near 3 MeV; similar to Fe an increase of strength was observed at low energy and shown to be in accord to a shell model calculation for M1-strength in the nuclides $^{94-96}\text{Mo}$ [sc13]. New photo-neutron data below 11 MeV [ut11] with smaller error bars and smooth dependence on E_γ replace the older ones [be71].

Quasi-elastic photon scattering from natural Sn has been studied long ago [ax70] at the tagging set up installed at Urbana and '*intermediate structure*' in addition to the IVGDR tail has been identified. The absorption cross sections were derived from scattering data [ax70]; their branching correction by inserting constant average resonance widths *may overestimate* σ_{abs} *by at most 20 %* [ax70]. To improve the overlap with the (γ, n) -data a reduction by 0.8 was applied when making Fig.10 and the resulting values are shown together with the cross section for $^{120}\text{Sn}(\gamma, xn)$ [le74], obtained with positron annihilation in flight; recently laser backscattered photons confirmed [ut11] these data.

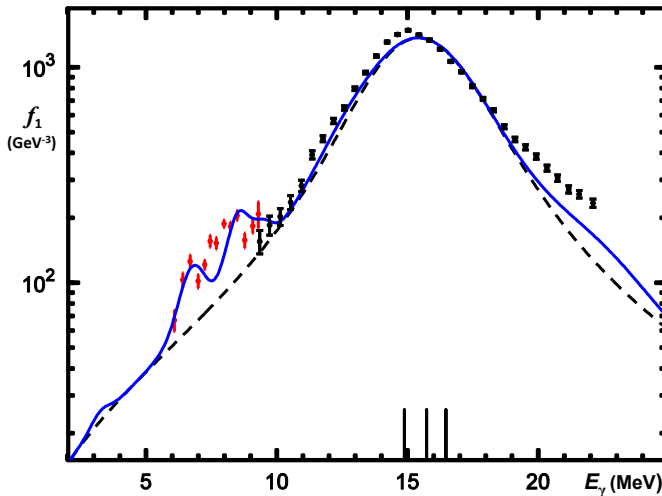


Fig. 10: Photon strength for ^{120}Sn from photon scattering (red \bullet [ax70]) at low and photo-dissociation (black \times [le74]) at higher energy in the IVGDR. The data are compared to TLO (black dashed line), the approximate influence of minor strength is depicted as drawn line in blue.

From a high resolution photon scattering experiment [go98] with correction for branching losses a strength enhancement near 6.5 and 8 MeV was reported for ^{116}Sn and ^{124}Sn , similar to what is shown here for ^{120}Sn . A recent study of ^{112}Sn and ^{120}Sn [Oe14] uses statistical corrections for inelastic scattering as proposed earlier [ru77] and again finds similar dipole strength as reported earlier. In addition the last-mentioned investigation has detected by a fluctuation analysis the need to increase the final photon strength by nearly a factor of two with respect to the sum of peaks observed in the spectra and resolved with ≈ 2 keV (FWHM) energy resolution. Data on f_γ derived at Oslo for other Sn isotopes with ^3He -induced reactions show significant differences from the photon scattering data shown here. The overshoot seen at the higher energies can be explained by the influence of the giant quadrupole resonance and is of no importance for radiative neutron capture.

Similar to what is seen in Fig. 9 (as well as in Figs. 7 or 8) an excess above TLO is indicated near $E_\gamma \cong 7$ MeV, i.e. at about 42 % of the central IVGDR-energy, and an enhancement of similar strength was also seen at an equivalent energy in ^{94}Mo [ro13]. The ‘*intermediate structure*’ strength seen below 10 MeV by photon scattering resembles the pigmy strength, since long observed [ba73, la79] in many heavy nuclei. Possible effects of and its contribution to the absorption cross section will be discussed later; it may be related to non-isovector E1-modes and, partially overlapping, M1-strength.

In Fig. 11 results from photo-neutron emission from ^{130}Te , multiplied by 0.9 – as done in general for data from Saclay – agree well to TLO. The necessary reduction may well be influenced by difficulties in the analysis of multi-hit events in the neutron detector array [va12, is04]. The low energy data support the finding of extra strength near $0.42 \times E_0$, but they also shed light on the difficulties arising in the analysis of scattering data heavily influenced by the incomplete knowledge of the ground state branching ratio.

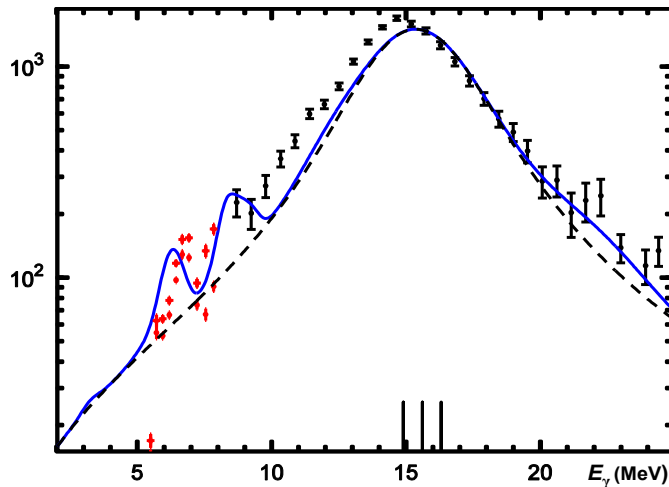


Fig. 11: Photon strength for ^{130}Te calculated as sum of three IVGDR-Lorentzians (black curve), and with minor strength added (blue) in comparison to data from photo-neutron production [le74] depicted as \bullet . The data below S_n (\bullet) are from a careful analysis [is13] of scattering data, yielding lower and upper limits for the photo-absorption cross section.

For ^{138}Ba scattering data have been taken with quasi mono-energetic photons at the laser backscattering beam at HIγS [to10], whereas an experiment at the ELBE bremsstrahl was performed with ^{136}Ba [ma12]. As one can assume that the two data sets result in very similar absorption cross sections, they are shown together in Fig. 12. A not yet confirmed and not shown increase below 3 MeV [ma12] may of similar origin as observations in Fe and for $N \approx 50$. In several heavy nuclei scattering experiments [po92, en09] with isoscalar He-projectiles have observed enhanced strength at $E_x \approx 0.42 \times E_{\text{IVGDR}}$ and its gamma-decay directly to the ground state such that an isoscalar mode was proposed to be a general feature [sa13]. For a globally applicable quantification discussed in that work the yield not seen as individual spectral lines with a Ge-detector (including the quasi-background) has to be determined with care and added [ma14].

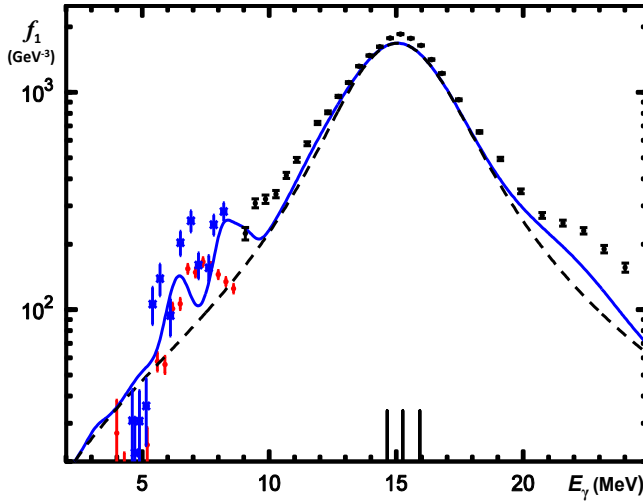


Fig. 12: Photon strength for ^{138}Ba derived by photo-neutron production (black squares [be71]) in comparison to TLO for the IVGDR (dashed curve in black). Photon scattering data for $E_\gamma < S_n$ are shown as blue squares [to10] and red squares (for ^{136}Ba [ma12], reduced by 0.7); for ^{136}Ba no data exist at $E_\gamma > S_n$.

For most of the isotopes to be discussed in the following (^{146}Nd to ^{238}U) photon strength information for $E_\gamma < S_n$ was obtained from individually known branching ratios of gamma transitions following neutron capture via resonances r [ba73] or by analysing primary gamma spectra following average resonance capture (ARC) [mu00]. The absolute photon widths can be derived from γ/n ratios and the resonance widths determined by neutron time of flight (tof). By an inspection of the gamma-ray angular distributions $\lambda=1$ is assured, if polarized neutrons are used the decay multipolarity (E1 or M1) is known experimentally [ko90]. Inserting these widths and the average level spacings into Eq. (14, right) results in $f_\lambda(E_\gamma)$, but this relies on a known level density $1/D_r$, and according to Eq. (14) this has lead us to an increase by 30% [ig06]. It is an open question to theory, if the dipole strength from such sources adds to TLO, what is suggested in the Figures.

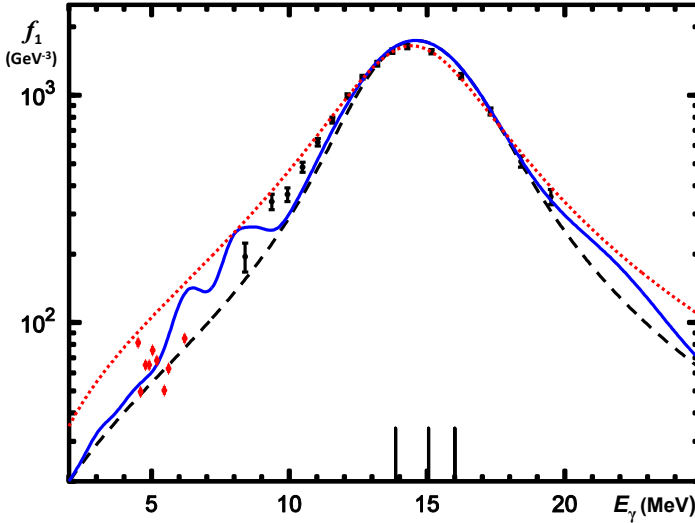


Fig. 13: The photon strength for ^{146}Nd in comparison to TLO for the IVGDR (dashed line in black). The data above S_n are from photo-neutron production [ca71] and the ones below are derived from gamma decay subsequent to ANC by ^{145}Nd [mu00]. The dotted line in red results from a fit to these data with one pole only [pl11] and the influence of minor strength is depicted as full line in blue.

In Fig. 13 the case of ^{146}Nd is shown and the regard of triaxiality in TLO leads to a reasonable description of data in the region of the IVGDR as well as below. In accord to Eq. (11) and (12) comparatively small Γ_k of 2.82, 3.33 and 3.76 MeV are used without a decrease with E_γ . In a previous work [be75, ca09, pl11] a single Lorentzian (SLO, $k=1$) was proposed for ^{146}Nd together with $\Gamma_{\text{IVGDR}}=5.74$ MeV, also shown in Fig. 13 as red curve. It indicates that such a fit leads to a large Γ , as it emphasizes the pole region. Only with a decrease of the damping or spreading width with E_γ^2 , as proposed [ca09] in EGLO, agreement to the low energy data near 5 MeV can be reached in spite of the large value for Γ . As ^{144}Nd and ^{146}Nd are considered an important cornerstone for the use of the underlying KMF-model [ko90] the success of TLO as presented in Fig. 13 challenges this model. As an experimental support of the KMF theory the data from $^{143}\text{Nd}(n, \gamma\alpha)$ were also quoted [po72, al77] – neglecting the fact, that there M1 radiation should be favoured [fu73], similar to what was indicated for $^{94-96}\text{Mo}$ [sc13]. In addition, the fact is ignored, that at $E_x < S_n$ the Fermi-gas relation between E_x and T is not adequate in many heavy nuclei, like in ^{144}Nd (cf. section IX). The global TLO also differs from other locally adjusted Lorentzians presented previously [ax70, be75, ut11] and TLO thus leads to conclusions at variance concerning eventual excess. The global adjustment of resonance width and strength in TLO makes the size of strength in the tail independent of the eventual differences in the IVGDR peaks. The fact, that for nuclei with magic nucleon numbers an improved description of the peak region is obtained by reducing the deformation somewhat has negligible influence in the tail region.

Enhanced photo-neutron cross sections 3-4 MeV below the peak have been observed in many nuclei [ex14] and the contribution to the dipole sum in Eq. (10) are small. In any case it can be stated that a decrease of Γ_{IVGDR} with decreasing E_γ as proposed [ka83, mu00, pl11] are in contrast to experiment – when global fit parameters are used as is done by TLO. Some enhancement near the energy of $0.42 \times E_{\text{IVGDR}}$ is seen in the data for ^{156}Gd shown in Fig. 14; they are selected as an example for experimental uncertainties to be aware of in discussions about details of the dipole strength: Two absorption experiments using rather similar

techniques [va69, gu81] disagree in the central IVGDR region beyond the ‘error bars’ published – not only in absolute but also in relative height for the two peaks, what does indicate an origin away from normalization or atomic background. No third data set is available and TLO comes close to an average of both publications, when a beam energy spread of 0.8 MeV (rms) is applied. The apparent disagreement of the two datasets covering the IVGDR peak can be viewed as an indication of the reliability of the (γ, n) data, many of which were obtained nearly 50 years ago.

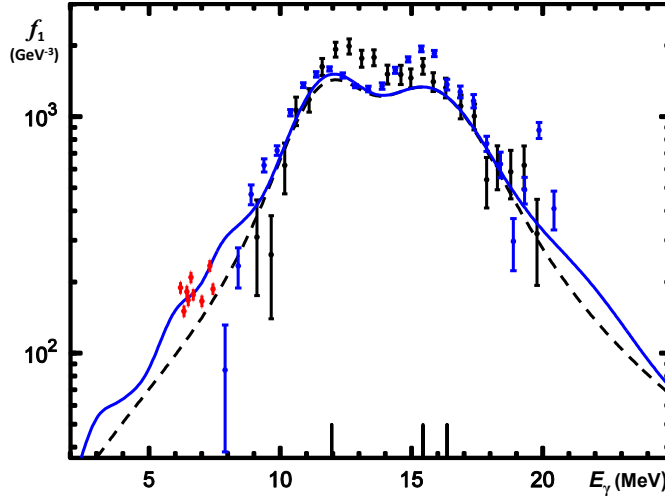


Fig. 14: Photon strength for ^{156}Gd in comparison to TLO calculated with (dashed black) and without (full line in blue) minor strength. Data are derived from ARC for 6-8 MeV (red \bullet) and from the cross section of photon absorption [va69] (blue \blacksquare) and [gu81] (black \blacksquare), which disagree in the peak area.

The ARC data included are subject to large Porter-Thomas fluctuations, which may be partly averaged by re-binning the plots. The acceptable agreement found when comparing the data to TLO, as can be seen in Figs. 14-16, is in contrast to the strong excess of the Lorentzian tail above the low energy data as reported previously for ‘non-deformed’ nuclei [mu00]. Again it is stressed here that TLO uses smaller (photon-energy independent) damping widths leading to a smaller strength in the tail region. In contrast, local fits neglecting triaxiality [ko90, ca09] suggest imposing an energy dependent width. As discussed by us in previous papers [ju08, ju10] this may bring the tail down considerably, and has a significant effect especially in the tail region below 9 MeV (see Figs. 10 & 24 and [ko90, Fig. 1 & 3]). With TLO this is avoided in conformance with the TRK-sum – near closed shells as well as for nuclei with large $|Q_0|$. There a small split between two poles (see Figs. 14 - 17, 20, 21) is hardly seen and Eq. (12) causes these two (and their sum) to have reduced height albeit all components have equal strength.

In Fig. 15 results of two different experiments on ^{168}Er for the IVGDR range are depicted: The data with the larger error bars were obtained [gu81] by photon absorption with subsequent subtraction of the strongly dominating absorption by the atomic system, which has to be determined by a precise calculation. As the other data [be68] stem from a photo-neutron experiment performed with a natural target, deviations might not be related to ^{168}Er . But still the agreement of both to TLO confirms the applicability of this parameterization.

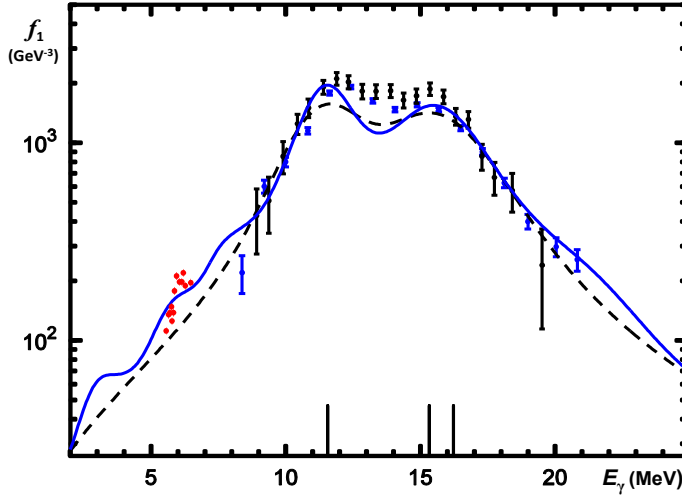


Fig. 15: Photon strength for ^{168}Er derived from ARC data (red+) and from the cross section of photon absorption (black +, [gu81]) in comparison to TLO (dashed curve in black). Shown as full line in blue is the prediction with minor strength, but without enhanced beam spread. Photo-neutron data for $^{nat}\text{Er}(\gamma, xn)$ [be68] are depicted as blue diamonds (\blacklozenge).

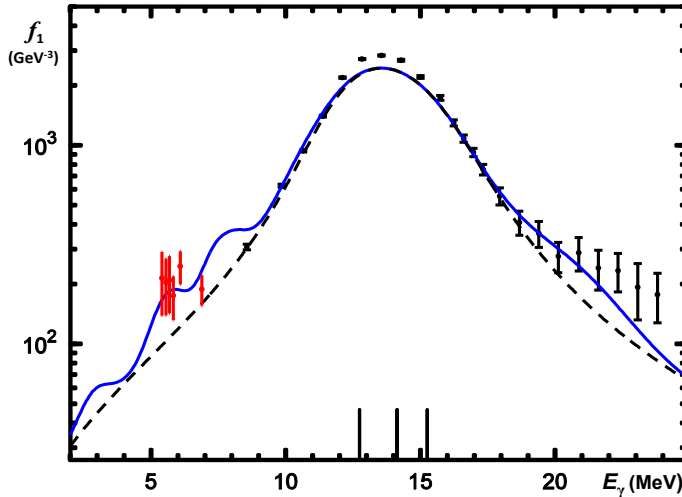


Fig. 16: Photon strength for ^{190}Os derived from ARC data (+, [ca79]) and from the cross section of photo-neutron production (+, [be75], positron annihilation). For comparison a TLO result is shown as dashed curve in black, the full line in blue contains minor strength components.

The photon strength as observed in photon scattering (Fig. 17 - 19) shows intermediate “pigmy” structure at $E_\gamma \approx 0.4 \times E_{IVGDR}$. Also the γ -decay observed after n-capture is reasonably well accounted for in TLO (Figs. 13 to 18), especially if an enhancement in the pigmy energy range is compared to the ‘minor’ strength proposed here. If summed, as parameterized in Table I, its contribution to the summed strength in Eq. (10) is weaker by at least one order of magnitude as compared to the IVGDR sum.

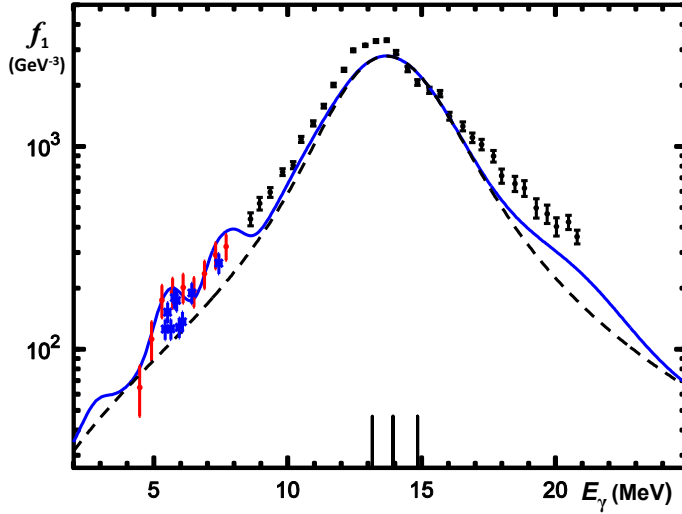


Fig. 17: Photon strength for ^{196}Pt derived from ARC data (+ [mu00]) and from the cross section of photo-neutron production (■ [go78]) in comparison to TLO (blue curve). Photon scattering data (red + [ma12] are reduced by 30 % in view of a ‘new’ ansatz for the level density [gr14].

Already many years ago, experiments with tagged photons [la79] have identified a resonance-like structure in the cross section of photon scattering on targets in the vicinity of ^{208}Pb , and the case of Hg is especially significant.

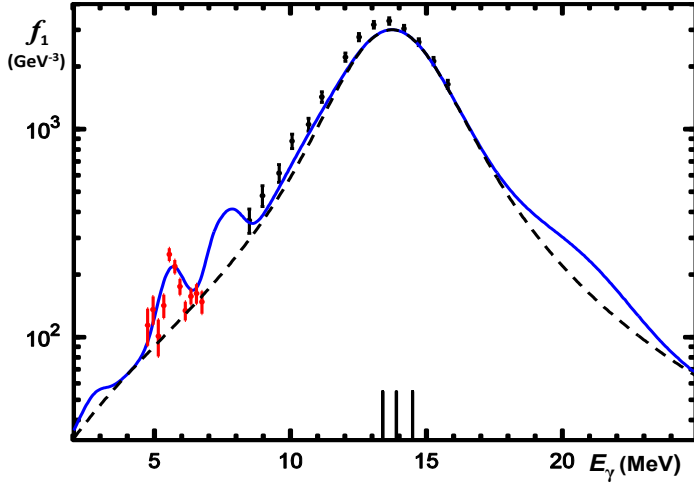


Fig. 18: Photon strength in ^{202}Hg calculated by TLO for the IVGDR, with (full line in blue) and without minor strength (dashed curve in black) is compared to photon scattering (■) [la79] or photo-neutron production (■) [ve70], respectively, both studied with ^{nat}Hg .

In ^{208}Pb this mode would lie in a region of small level density and hence very large spacing between 1^- -levels and it is intriguing to relate this prediction to the strong 1^- -level at 5.51 MeV [pi09, sc10] and eventually weaker ones seen nearby in this region of low level density $\rho(E_x)$. This rather small $\rho(E_x)$ reaching up to the IVGDR range is related to the large shell correction in near-magic nuclei as will be discussed in section VIII. Thus Porter-Thomas fluctuations have a strong influence on the data leading not to smooth strength function curves – in contrast to the approximate prediction used here. For ^{208}Pb several investigations [ve70, vy78, be82, na91] have explicitly looked at fine-structure at $E_x < 12$ MeV and some fluctuations in excess of the smooth IVGDR slope are seen; these are partly smeared out in the figures. Indications of contributions from the GQR are also observed; unfortunately

related electron scattering data [bu72, pi74, ku81] do not allow a fully consistent transfer of information. Inelastic proton scattering [dj82] indicates a peak at 21.5 MeV which could be either IVGQR or IVGMR, whereas the ISGQR is indicated in Figs. 13 – 19 to partly overlap one or two of the IVGDR components. This excess over TLO contributes less than 5 % to Eq. (10) and also the pigmy addition contributes not more. Corrections of photon scattering yields have been performed using inelastic photon scattering data taken at the Urbana microtron laboratory [la79], where also the neutron emission directly to low levels of ^{207}Pb was observed [be82]; it is of minor importance for the arguments discussed here.

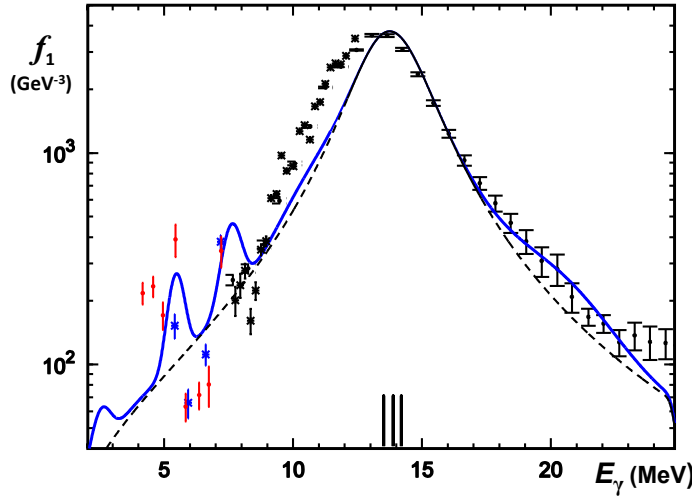


Fig. 19: Photon strength for ^{208}Pb derived from photon scattering data using a quasi-monochromatic beam (●, [la79]), from bremsstrahlung (↓, [sc 10]) and from two cross section measurements for photo-neutron production (◐[ve70], * [vy78]). TLO for the IVGDR is depicted as dashed line in black; GQR and minor strength was included for the full line in blue.

In Fig. 20 and 21 three sets of experimental data for ^{232}Th and ^{238}U , respectively, in the range of the IVGDR are displayed together: The data with the large error bars were obtained by photon absorption with subsequent subtraction of the strongly dominating absorption by the atomic system, which has to be determined by a precise calculation. They agree within uncertainty to data stemming from a photo-neutron experiment performed at Saclay, which were thus reduced here by 10 %. The agreement is not perfect, but indicates the reliability of both in the IVGDR regime.

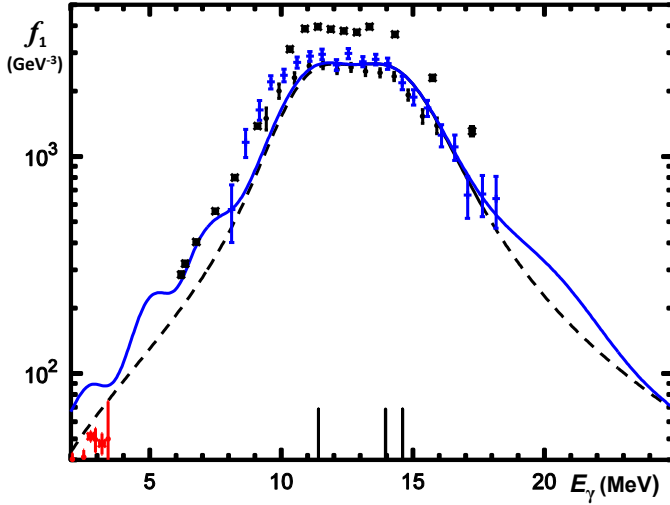


Fig. 20: Photon strength for ^{232}Th derived from photo-neutron production cross sections from Saclay (+, [ve73]) and from Livermore (*, [ca80]); both include (γ, f) . Photon absorption data (●, [gu76]), which disagree to the latter and to TLO (dashed black for the IVGDR, full line in blue includes minor strength). Data from γ -decay after He-scattering (*, [gu14]) are included at low energy.

The accord between two data sets is important with respect to the disagreeing data obtained at Livermore [ca80]. These cross sections for ^{232}Th and ^{238}U are exceptional large in the sense, that an analysis on the basis of Eq. (10) indicates an overshoot of $\gtrsim 30\%$ as compared to the TRK sum.

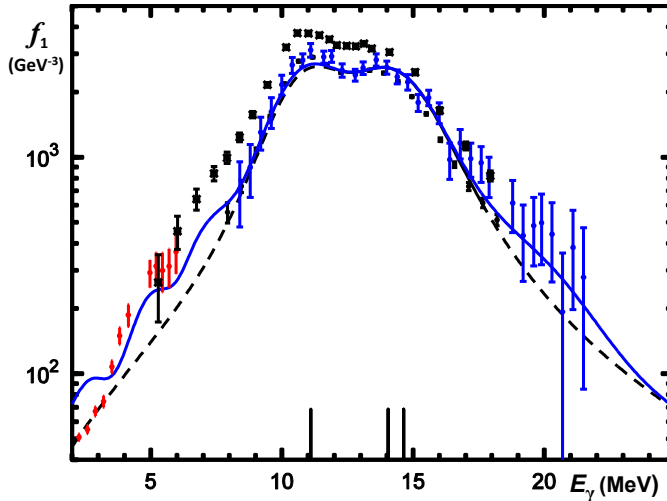


Fig. 21: Photon strength for ^{238}U predicted by from TLO for the IVGDR (black curve) and including minor strength (blue) in comparison to two differing sets of data derived from the cross section of photo-neutron production (+, [ve70], □, [ca80]); both include (γ, f) . Also shown are photon absorption results (●, [gu76]) and data from photon scattering (■, [ba73]) using a quasi-monochromatic beam. Data from γ -decay after deuteron-scattering (*, [gu14]) are included at low energy.

The pigmy mode seems to be present in photon scattering by all nuclei studied with $A > 70$. For lower energies the scissors mode was predicted [he10] to also be a general feature in all heavy nuclei, but in photon scattering it is difficult to separate from the E1 strength originating from quadrupole-octupole coupling. Results for a strong M1 mode presented recently [gu14] suffer from the missing parity assignment of the strength observed as well as from a questionable choice for the IVGDR tail. An identification as M1 is well possible by

comparing e- and γ -scattering [he88] and respective results indicate some difference to data from inelastic deuteron scattering [gu14] suggesting further study.

For all nuclei investigated here a quite good agreement between observations and the TLO prediction for the E1 strength is found. TLO relies on the classical sum rule (TRK), the IVGDR mode energies E_0 are derived from the droplet model and a width Γ varying with it and hence slowly with A and Z . There is no dependence of it on E_γ , but on the three sub-mode energies E_k , which are derived from the deformation dependant axis parameters determined by CHFB calculations [de10]. There is one deficiency apparent in these: In nuclei with or near closed shells the calculations predict more deformation [be07] as deduced from $B(E2)$ -values and, as found within the study presented here, in disaccord to the deformation induced splitting of the IVGDR. For closed shell nuclei a small deformation (reduced by a factor 0.4 to 1 as described together with Fig. 6) results in a better description of the IVGDR peak shape, and this reduction has no significant influence on the strength in the tail region, which will be shown to be essential for radiative capture. It is worth mentioning here that the experimental data below S_n for isotopes used as an argument for parameterizations other than TLO [ko90, mu99] can well be described by TLO. Also an account for the variance of the deformation parameters by instantaneous shape sampling [zh09] only leads to small changes of the calculated shapes for the IVGDR in deformed nuclei: The resonances are widened near the peak region, but the low energy tail remains unchanged. In closed shell nuclei and their neighbours the low level density induces narrow variations in the cross section data up to energies near S_n . These are eventually identified as a second type of pigmy resonances [zi05]; their contribution to the summed cross section stays below a few per cent. In general, the following conclusions can be drawn from the comparison of experimental data to Eqs. 11 and 13 as depicted here for 20 nuclei in the mass range from 50 to 250:

- a. The centroid IVGDR energies derived from droplet model fits to masses [my77, mo95] are in accord to the data, when an effective mass $m_{\text{effc}}^2 = 800$ MeV and the neutron radii as predicted from the CHFB calculations [da10] are used.
- b. There is no indication of a strong departure from the classical dipole sum rule [ku25, ge54] if the yield above the IVGDR is identified to the quasi-deuteron strength. Previous reports on deviations are likely to be due to overestimated resonance widths resulting from an *ad hoc* limitation to axial symmetry.
- c. The resonance widths vary only smoothly with A and Z and only via the power law dependence (*cf.* Eq. (12)) of the IVGDR width on the resonance energy, which is predicted by hydro-dynamical considerations [da58, da64, bu91, na91] in accordance to experimental data [en92].
- d. The IVGDR data together with data obtained with different methods for lower energies do not allow for a strong decrease of the width with photon energy, as previously postulated [ka83]. Again, with the high width values as used in the past [be75, di88, pl11] this may have served as a means to compensate the otherwise large strength at low energy.
- e. Three rather narrow resonance parts add up to a wide structure and make a large spreading width superfluous. Only by allowing a broken axial symmetry, which is not

- obvious by the need of a three-pole fit, a satisfying splitting of the IVGDR is reached; this indicates the importance of calculations [de10] or other input [ju08].
- f. Experimental data suffer from missing exact information on resolution as well as on detection efficiency, both obvious through differences between laboratories.
 - g. Parameterizations become more reliable, when data from different experiments are combined and discrepancies suppressed – as was proposed for the case of ^{232}Th and ^{238}U , where the agreement to TLO is remarkable for such heavy nuclei.

The comparisons of a very similar ansatz to a number of other isotopes as published previously [ju08, be11, sc10, na08, er10, sc11, na10, ju10, gr10] can also be considered here, such that a nearly complete sample of IVGDR data in heavy nuclei are well described by TLO. A description of the IVGDR in deformed nuclei [ma05] not using the TRK sum rule and not based on a fully self-consistent calculation of the shape parameters was by far less successful in its predictions.

VII. Special considerations for odd nuclei

For neutron s-wave capture on $J=0$ targets it has been shown [gr14] that the TLO ansatz also works for the odd nucleus ^{89}Y . When an average over the axis lengths for even neighbour nuclei is used to obtain $f_{\text{E}1}$, a good description for the IVGDR region is obtained. It was assumed, that for $J_0 \neq 0$ photon absorption into a mode λ populates m members of a multiplet with $m = \min(2\lambda+1, 2J_0+1)$ and the decay widths to the ground state $\Gamma_{0\text{r}}$ are equal for each member of the multiplet, and that the conditions for the validity of Eqs. 13 and 14 are thus fulfilled. The strength observed corresponds to the cross section summed over the multiplet and this can be described by an effective g , which in accord to Eq. (3) is:

$$g_{\text{eff}} = \sum_{r=1,m} \frac{2J_r+1}{2J_0+1} = 2\lambda+1. \quad (15).$$

This ansatz is valid in heavy nuclei [ba73] as it relates to the condition of weak coupling between the odd particle and the mode λ . The TLO-calculations for odd- A nuclei as shown in Figs. 22-24 were performed on the basis of Eqs. (13 -15) with $k=1,2,3$.

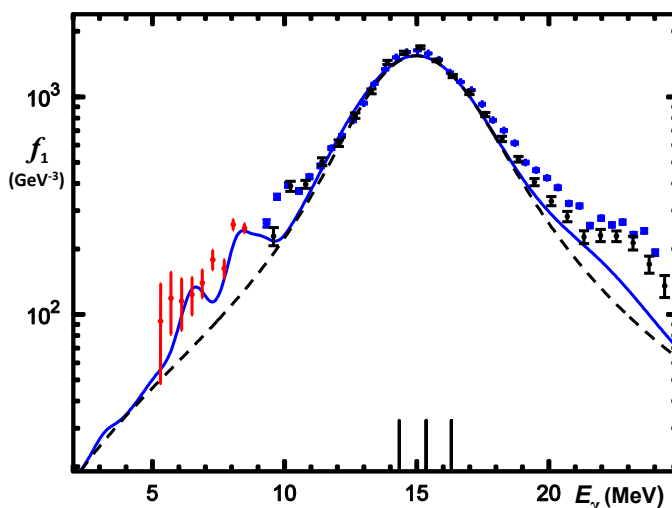


Fig. 22: Photon strength for ^{133}Cs calculated as sum of three IVGDR-Lorentzians (full black curve), and with minor strength added (dashed curve in blue) in comparison to two datasets of photo-neutron

production shown as \perp [be69] and \times [le74]. The photo-absorption data below S_n (\dagger) are derived from elastic scattering by the neighbour nucleus ^{132}Xe [ma14], reduced by 30%.

No extra spin dependent factors are needed and agreement to the experimental data is found to be similar as in the case for even nuclei, also in the tail region below S_n . In Fig. 22 data for ^{133}Cs are shown to be close to those for neighbouring even nuclei depicted in Figs. 12 and 13. The agreement to TLO is obvious and also ‘minor’ strength as pigmy and the IVGQR are seen.

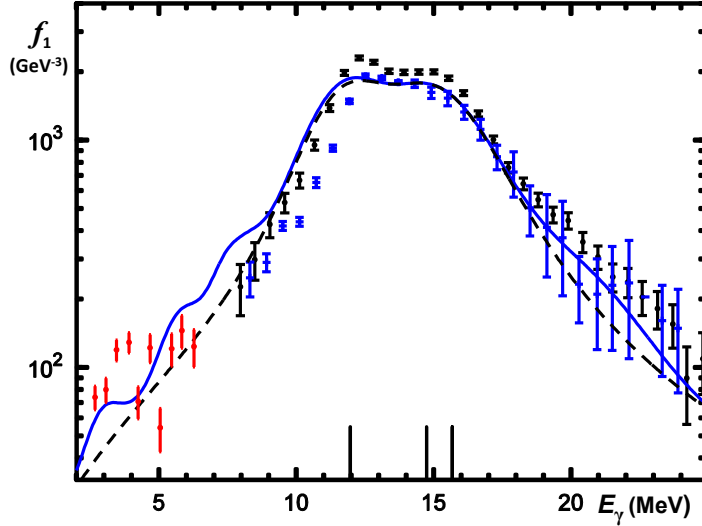


Fig. 23: Photon strength derived for $^{181,2}\text{Ta}$ from photon scattering (\bullet , [ma14]), ARC data (\dagger , $^{181}\text{Ta}(\text{n},\gamma)$ [mu00]) and from photo-neutron production ($^{181}\text{Ta}(\gamma,\text{xn})$ \ddagger , [an67]; \perp , [be68]) in comparison to TLO in ^{182}Ta (black curve for IV-E1, blue including minor strength).

For the odd mass ^{197}Au not only the prediction is depicted, but also a SLO curve from RIPL-3 [ca09, pl11], which clearly over-predicts the data below S_n extracted from Fig. 18 of ref. [ba73]. In contrast to the missing strength as compared to a single Lorentzian used there, the agreement is reasonable for TLO, when the discontinuity near 19 MeV is related to the known incorrect separation of the 2n-channel.

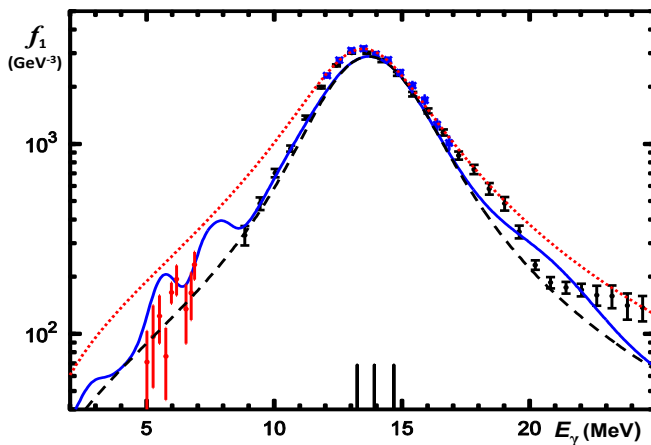


Fig. 24: Photon strength for ^{197}Au derived from photon scattering data (\square , [ba73]) using a quasi-monochromatic beam and from the cross section of photo-neutron production (\bullet , [ve70]) in comparison to the TLO prediction for the IVGDR (dashed curve in black); the full curve in blue results from the inclusion of minor strength. Also shown are newer data for the peak region (\ast , [be78]) together with a SLO fit curve from RIPL-3 [pl11] (dotted in red).

This change is due to the inclusion of triaxiality in TLO, which leads to a reduction of Γ_k and thus of σ_{abs} for sufficiently large $(E_k^2 - E_\gamma^2)^2$ in Eq. (11). The Γ_k used previously [ba73] are 2.9 and 4.0 MeV and an additional factor of 1.22 was obtained as compared to the TRK-sum. This extra factor is not needed by TLO and the values for Γ_k are 2.7, 3.0 and 3.5 MeV. When $^{197,8}\text{Au}$ is considered spherical $\Gamma \approx 4.5$ MeV results from a SLO-fit and this effects largely the strength predicted in the tail region [gu81, ko90]. Also for ^{197}Au the use of the KMF-model was proposed [ko90] and the success of TLO as presented in Fig. 24 challenges this model again.

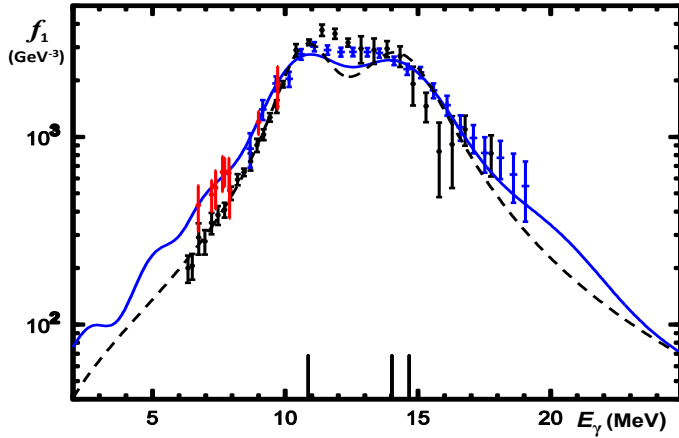


Fig. 25: Photon strength for ^{239}Pu (black dashed curve: TLO without enhanced beam dispersion; full blue curve: minor strength added to TLO, assuming beam dispersion enhanced to 0.8 MeV). Data are derived from summing cross sections of fission and neutron production induced by bremsstrahlung (\bullet , [gu76]) and quasi-mono-energetic photons (\square , [be86]). The data in red (\bullet , [mo93]) on the low energy slope were obtained with neutron capture γ -rays.

In the bombardment with photons ^{239}Pu mainly undergoes fission and the weaker neutron emission channel has to be added to obtain σ_{abs} . In Fig. 25 the result of this sum of Livermore data [be86] is compared to two sets of direct absorption data and a reasonable agreement is seen, as well as a good accord to the TLO-prediction. This is remarkable in view of the disagreements depicted in Figs. 20 and 21 for the near neighbours ^{232}Th and ^{238}U and doubts about these data seem affirmed. Together with the agreement between ^{88}Sr and ^{89}Y reported recently [Gr14] the examples presented in this section support the actual ansatz for the derivation of photon strength for odd nuclei.

The assumption made for TLO that the damping widths Γ_k do only depend on E_k and not on E_γ clearly is at variance to previous proposals made for the electric dipole strength function [ko90] and recently made [ca09] modifications of this work. Following the so-called KMF approach [ka83] a prediction was made for the dipole strength at energies far below the giant resonance with a quadratic dependence of the spreading width on photon energy and on the temperature T at the final level. To arrive at a combined formula for the full energy range the additional assumption is made – based on arguments derived from Fermi liquid theory [ka83] – that this spreading width coincides with the IVGDR damping width at its pole energy E_0 [ka83]. The T -dependent component is added to the Lorentzian at low energy for the γ -decay calculation only and this violates the Axel-Brink hypothesis. Several comments should be made concerning this ansatz:

An average overshoot of 20-30% over the TRK sum rule results from the disregard of triaxial deformation when fitting IVGDR data.

- (a) This is connected to the large widths extracted (cf. Fig. 4) which also leads to an increase of strength predicted at small excitation energy.
- (b) This increase seems to be somehow compensated by (a), (b) and a postulated decrease of the IVGDR width with photon energy, as is usually assumed [ko90].
- (c) A continuous strength below 1 MeV, observed [po72], but never identified experimentally as E1, is often added to counteract this decrease.

It seems, that Fermi liquid theory has to be investigated again concerning its use for the evaluation of photon strength, and a respective attempt was published previously [mu00]. The parameterization proposed in the present work obeys the Axel-Brink rule and hence differs significantly; it results in a relation between the IVGDR extrapolation and photon strength, now on the basis of TLO, and is a novel example for their useful combination.

VIII. Photon strength of other character than isovector electric dipole

The height of the low energy tail, of special importance for predictions of radiative width and hence for radiative capture cross sections, is nearly proportional to the IVGDR width and it depends weakly on its deformation induced splitting. An explicit photon energy dependence of the IVGDR width as introduced as modified Lorentzian (MLO) in the Parameter Library RIPL-3 [ca09] results a considerable modification of the prediction in the low energy tail [ju08]. But literature on photon scattering in this energy range has pointed out the possible importance of strength of other character than isovector electric dipole, as recently reviewed [gr12], and in the following also work published more recently is included. The discussion will be generalized to electromagnetic strength of different character; even if it has minor importance for photon absorption and the sum rules, it may influence the decay of the compound nucleus and consequently also the reaction cross sections. Strength eventually adding to the IVGDR tail is characterized by approximate expressions listed in Table I and its possible importance will be investigated. The direct relation between ground state transition widths, in fm^2 and summed within an interval Δ_E (given expressed in MeV), and the f_{λ} (in $\text{GeV}^{(2\lambda+1)}$) as derived from Eqs. 13 and 14 can be used to extract strength information from summing spectroscopic width data over a given energy range Δ_E :

$$f_{\lambda}(E_{\gamma}) = \frac{1}{\Delta_E} \sum \frac{\Gamma_{r\gamma}}{E_{\gamma}^{2\lambda+1}} = \frac{I_{abs}^{\lambda}}{(\pi\hbar c)^2 g_{eff} E_{\gamma}^{2\lambda-1} \Delta_E} \quad (16).$$

The second part of Eq. (16) allows to relate the strength function to integrated absorption cross sections; these can be directly related to sum rules assumed to be valid independent of spectroscopic details, known to exist in certain regions in the nuclide chart.

Electric dipole strength below the IVGDR

Long ago a low energy dipole mode was predicted to be formed by E3 strength coupled to low energy quadrupole modes [bo57]. In many even-even nuclei rather strong photon absorption into 1^- -levels with $1 \text{ MeV} < E_x < 4 \text{ MeV}$ has been observed [kn95] and a correlation of E_x to the sum of the excitation energies of the low collective 2^+ and 3^- -modes was established. A systematic dependence of this dipole strength on A and Z has not been

registered, probably due to possibly destructive interference between different contributions [an01]. A functional dependence proposed for the $2^+ \times 3^-$ -mode from theoretical arguments [bo57] was further specified [ko05, kn06] and the B(E1)-values predicted are in the range of observations in nuclei of various degrees of deformation. Photon scattering studies show similar strength for odd and even nuclei with varying deformations [kn95], but the missing of small components of strength, more fragmented away from closed shells and especially in odd nuclei, cannot be excluded. To estimate the influence of this low energy electric coupled vibrational dipole mode on the photon emission a Gaussian distribution is considered as an approximation, with parameters listed in Table I. The centroid energy E_{q0} is taken as the sum of the energy of the 1st 2^+ -level [ra01] and the corresponding value for the octupole (3^-) excitation [ki80]; theoretical approximations for exotic nuclei are available [de10, ro11].

In principle Eq. (16) would allow the inclusion in this study of numerous recently published results for strength not far below S_n and hence near 7 MeV. In case an assignment to E1 is made, it is often denoted as *PDR* ('*Pygmy Dipole Resonance*') [ry02, sa13], and eventually assigned to the '*vibration of excess neutrons against a proton–neutron core*', or also as '*an integral part of a toroidal E1 mode representing an example of vortex collective motion in nuclei*'. '*Intermediate structure*' in photon scattering was discussed in detail [ba77] and the concept of photon strength functions $f_\lambda(E_\gamma)$ was then introduced. At energies approaching S_n an extraction of $f_\lambda(E_\gamma)$ from photon scattering data becomes questionable when competing channels suppress the emission of elastic photons and often unobserved decay branches (inelastic photon scattering) are not easily accounted for. This may fake a fall-off which, together with the rise when approaching the IVGDR, appears as a peaking distribution. The main strength in that energy range identified in the isotopes $^{112-124}\text{Sn}$ [go98, oe14] by high resolution γ -spectroscopy allowed to estimate the full dipole strength by accounting for additional quasi-continuum contributions and the loss due to branching. Its peak energy increases weakly with decreasing A, but no clear change of the integrated strength is observed, even when combining it with data for ^{138}Ba and ^{140}Ce [en09] and recent work for Xe-isotopes [ma14]. Concerning the observations on seemingly isolated peaks in gamma spectra extra care is indicated: It was shown that Porter-Thomas fluctuations may sham structures in data taken with a resolution larger than the level distance and thus not sufficient to resolve all levels [ha90]: *Sampling will give many small numbers and a few large ones and this is ideally suited for providing the pronounced peak structure that makes for the happiness of every dyed-in-the-wool spectroscopist.*

In a few earlier papers this problem was addressed experimentally with other photon detectors and strength data were given for structure in photon scattering by Zr and Sn [ax70] as well as for $A \approx 200$ [la79] in the region between 5 and 6 MeV. As mentioned there, the contribution of the quasi-continuum below the lines should be included after the real background due to unwanted radiative processes in the detector and the near-by environment has been quantified and subtracted. In the limit of $E_\gamma \rightarrow 0$ the strength f_{E1} is expected to vanish, as suggested by the well-known fact that nuclei do not have an electric dipole moment [bo75, st05], but this may be hidden by Thomson scattering dominating at long wavelengths. Fragmented parts of the electric dipole strength outside of the IVGDR may have isovector or isoscalar character and a distinction by experiments with isoscalar beams was proposed [po92, en09, sa13]. This

approach is not unambiguous, as only in collective models based on one incompressible fluid isoscalar electric dipole strength is isospin forbidden as it would correspond to a spurious motion of the centre of mass [bo57, ha02]. Hints for the isoscalar character of electric dipole strength may indicate non-uniform proton-neutron distributions or compressional modes. Strength between $E_x \cong 5.5$ MeV and the neutron separation energy S_n was shown to be of isoscalar nature in ^{40}Ca , ^{58}Ni , ^{90}Zr and ^{208}Pb by the coincident observation of inelastically scattered α -particles and de-excitation γ -rays [po92].

In the present study the various results reported for this energy range are considered an addition to the TLO-extrapolation and tentatively separated into two components named low and high energy pigmy mode in Table I; by this means it is assured, that the total strength included may be understood as an upper limit. In Figs. 7 to 25 the strength of seemingly resonant strength near $0.4 \times E_{\text{IVGDR}}$ appears to be similar in its sum for many different A , when compared to the IVGDR. Hence this intermediate structure resembles to a prediction made for ^{208}Pb : In a three-fluid hydro-dynamical model of heavy nuclei [mo71] an oscillation of the excess neutrons against a core with $N=Z$ was shown to result in a peak of energy $E_x \lesssim 0.4 E_0$. The full vibration of the neutrons against the protons, the IVGDR [go48, st50, my77] leads to a dipole resonance at higher energy E_0 . Experimental ‘*evidence for a 5.5-MeV radiation bump*’, an intermediate structure then named ‘*pigmy*’ [ba73], suggested to look for a common description of it valid for all heavy nuclei. Independent of the possible manifestation as nuclear halo oscillation an approximation based on a Gaussian seems justified for the nuclei studied here. Resulting parameters for this low energy pigmy mode are given in Table I, and these values are in rough accord to many data the TLO-integral over the energy interval is subtracted [ma14]; thus they are purely phenomenological and independent of models proposed in view of data showing ‘*pygmy strength*’ [sa13].

Magnetic dipole strength

For both dipole modes (E1 and M1) Eq. (16) can be used together with the generalization of Eq. (9) to gather strength information from spectroscopic data. Here, the squared reduced matrix elements are inserted, which are direction independent at variance to the still often used $B(E\lambda)$ values. They are expressed in fm^2 .

$$\Gamma_{r0}(E_\gamma; E, M1) = \frac{16 \pi}{9} \frac{\alpha_e E_\gamma^3}{g(\hbar c)^2} \cdot |\langle r || \mathbf{E}, \mathbf{M} 1 || 0 \rangle|^2 \quad (17).$$

The photon strength between nuclear ground states and the IVGDR region is predominantly of electric dipole (E1) character and also in the tail region around 5 MeV M1 decays are weaker as compared to E1 [ko90]. Magnetic (M1) spin flip strength occurs at higher energy than collective orbital magnetic strength (scissors mode), which is strong in nuclei with large quadrupole moment and possibly contributes to radiative capture. Both built either on ground states or on excited levels and then contribute to the strength on top of them [kr13] in the sense of the Axel-Brink hypothesis. High resolution photon scattering data as *e.g.* published by [en09] show spectral details indicating low level density, which are especially significant in near magic nuclei. Again weak components at low energy are likely to be hidden in a quasi-continuum partly due to experimental background. Combined measurements of transition rates and polarization in the gamma decay of compound nuclei have been

performed e.g. for $A = 79$ [sc88] and the strength of low energy M1 transitions has been determined to be lower than for E1 in general. But measurements are rare for statistically significant ensembles of transitions in one nucleus. A possible way out is to average over many nuclei and a suitable compilation [so12] is available and updated regularly.

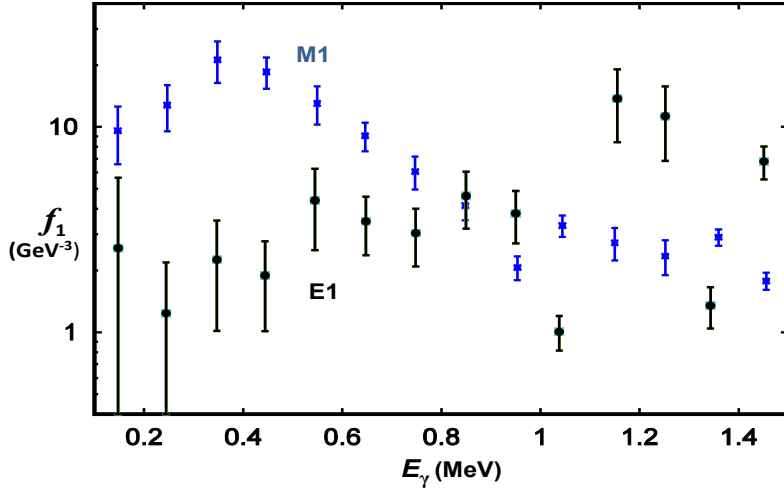


Fig. 26: Strength functions for an ensemble of nearly 3000 transitions in heavy nuclei with $80 < A < 180$ as extracted from a data compilation [so12]. The vertical bars indicate 20% of the root-mean-square of the distribution of the data in each bin and the points depict the averages for M1 (blue \diamond) and E1 (black \bullet).

The sorting of nearly 3000 transitions from compiled data [ex14] for $80 < A < 180$ has resulted in the plot presented in Fig. 26. The $f_{M1}(E_\gamma)$ are apparently considerably larger than $f_{E1}(E_\gamma)$ for E_γ below 1 MeV whereas above the E1 strength becomes stronger up to the region of the IVGDR. A direct measurement of the transition strength contributing to the decay width in the high level density region near S_n was possible by using experimental information gained in $^{143}\text{Nd}(n,\gamma\alpha)$ experiments [po72, al77]. In view of Fig. 26 this ‘low energy’ strength is likely to be mainly M1 as pointed out before [fu73], but E1 was occasionally assumed to be the main component [ko90]. In any case the summed dipole strength function f_1 in this mode was shown [po72, sc13] to be small and concentrated at very small E_γ and will not be added to the TLO-parameterization presented and used here. Although such a low energy M1-component has been used [ko90, ko08] eventually, it may be considered unimportant for the prediction of radiative n-capture, as the compilation of experimental data shown in Fig. 26 depicts a strong decrease for $E_\gamma \gtrsim 1\text{ MeV}$. Recently predicted very low energy M1 transitions resulting from orbital rearrangement occur mainly at high excitation [sc13].

In a recent review [he10] the properties of three components of magnetic dipole strength have been described in detail: For energies between 2 and 4 MeV orbital M1 strength has been observed, and it has been shown that with increasing ground state deformation β this orbital scissors mode reaches an integrated strength proportional to $Z^2\beta^2$ at an excitation energy $0.21 \cdot E_{\text{IVGDR}}$, in accord to data reviewed recently [en05]. The enhancement of gamma decay between high lying levels as observed in two step cascades [kr04, si06] was attributed to orbital scissors mode of about the strength seen by photon scattering. As shown [he10] the “*spin strength represents the largest fraction of the M1 strength*”, and for the energy range around $41 A^{-1/3}$ MeV a double humped structure is seen, identified as isoscalar and isovector spin-flip modes. This is in accord to the strength observed in heavy nuclei with polarized

neutrons [ko90]. Including both regions at $\sim 34 \text{ A}^{-1/3} \text{ MeV}$ and $\sim 42 \text{ A}^{-1/3} \text{ MeV}$ [he10] the energy weighted sum can be calculated within the energy range Δ_E with reasonable accuracy; it reaches $\lesssim 2 \text{ MeV fm}^2$, as the A-dependence of peak energy and peak integral approximately compensate each other [he10]. The resulting estimate is smaller by at least 2 orders of magnitude as compared to the main component [ge54, eq. 5.6] of the GGT sum rule obtained from very general arguments for the total photon strength in heavy nuclei, *i.e.* including all multipolarities. In the work presented here the scissors mode is considered as well as the two spin-flip M1 components, which are becoming important at higher photon energy. Polarization data are necessary to identify magnetic strength unambiguously and observations made with polarized photons on ^{88}Sr [sc07] and ^{90}Zr [la87] were performed at two different laboratories and with two different techniques: off axis continuous bremsstrahlung and tagged photons. A rather high magnetic strength was recently applied in Zr-isotopes [ut08], although it superseded the systematics [he10] by a factor of ≈ 3 , and combined to the rather low E1-strength as derived from a HFB+QRPA calculations [gy04] resulting in a suitable agreement to capture data; in view of the M1-enhancement needed the underlying E1model may have to be revised.

Electric quadrupole modes:

Low energy E2- transitions can be considerably enhanced and have played an important role in the spectroscopy of heavy nuclei – as discussed in sections II and III. The photon absorption cross sections can be derived from Eq. (3); they have been found to be small as compared to E1 excitation [we80] in the energy region near S_n . In Fig. 7 to 25 f_{E2} was multiplied with E_γ^2 , the additional energy dependent phase space factor for absorption and decay, to allow a visual comparison to f_1 ; but by using Eq. (8) for the integral $I_{E2} = I_c$ (as listed in table I) the correct decay width is used in the calculations. At variance to previous work [we80, ju08, ca09, ru13] the influence of quadrupole giant resonance (QDR) contributions to photon absorption is investigated; information for quadrupole strength comes from sum rules and theoretical predictions [na65, we80, wo91] adjusted to electron scattering data [pi74, sc75, do82]. The isoscalar ISGQR lies not far from the pole of the IVGDR such that it adds to the strength extracted there from data. Strength modifications due to the IVGQR appear to be important, as seen in Figs. 10-25, and result in a difference from TLO at higher energy. The influence of low energy quadrupole modes is investigated by assuming 5 % of the ISGQR integral $\int \sigma_{\text{abs}} dE$ to be downshifted by a factor of three in energy.

Using the abovementioned information and data [la87, ko90, he10] for the integrals of the E1, E2 and M1 components an approximation evolves for the ‘minor’ contributions to the photon strength function, which are inserted as listed in Table 1, where some of the components (*e.g.* M1 and ISGQR) have been enlarged as compared to literature values to assure that an upper limit is used in the subsequent estimates for the influence of ‘minor’ modes on the photon emission. Separate Gaussian distributions:

$$f_\lambda(E_\gamma) = \frac{1}{(\pi\hbar c)^2 g_{\text{eff}} \cdot E_\gamma^{2\lambda-1}} \cdot \frac{I_c}{\sqrt{2\pi}\sigma_c} e^{\frac{-(E_\gamma - E_c)^2}{2\sigma_c^2}} \quad (18)$$

for each of them are used to avoid unwanted strength in long tails. No arguments could be found, why Lorentzians should be preferred; this is contrast to the IVGDR, where a

Lorentzian with energy independent width is appropriate [do72, go77]. The I_c in Eq. (18) as well as in Table I are sums over many individual levels within the Gaussian width σ_c like in Eq. (11) for the IVGDR and in contrast to Eq. (7), valid for a single level.

Component \ parameter	E_c	I_c	σ_c
& multipolarity \ units	MeV	fm ² MeV	MeV
low E_x pigmy mode, E1	$0.43 \cdot E_0$	$7 \cdot Z \cdot (N-Z)/A$	0.6
high E_x pigmy mode, E1	$0.55 \cdot E_0$	$13 \cdot Z \cdot (N-Z)/A$	0.5
$0^+ \leftrightarrow (2^+ \times 3^-)_{1^-}$	$140/N(1+107/Z)$	$0.006 \cdot ZA \cdot \beta$	0.6
orbital M1 (scissors mode)	$0.21 \cdot E_0$	$0.033 \cdot (Z\beta)^2$	0.4
isoscalar spin-flip M1	$42 \cdot A^{-1/3}$	17	0.8
isovector spin-flip M1	$47 \cdot A^{-1/3}$	27	1.3
low E_x E2-modes	$19 \cdot A^{-1/3}$	$0.1 \cdot \alpha_e \cdot (\pi R_p E_\gamma)^2 \cdot Z^2 / (3 A m_p c^2)$	1
ISGQR, E2	$63 \cdot A^{-1/3}$	$2 \cdot \alpha_e \cdot (\pi R_p E_\gamma)^2 \cdot Z^2 / (3 A m_p c^2)$	1
IVGQR, E2	$48 \cdot A^{-1/6}$	$\alpha_e \cdot (\pi R_p E_\gamma)^2 \cdot ZN / (3 A \cdot m_p c^2)$	1.8

Table I: Parameters of an upper limit for two minor electric and three magnetic dipole modes to the dipole strength function to be calculated with a Gaussian (Eq. 19). An equivalent shape near the peak is reached for a Gaussian with a rms width, which is larger by 2.5 as compared to the width Γ of a Lorentzian. Two GQR modes are listed, which are also seen in photon absorption; they are proportional to the square of the nucleus' charge radius R_p (rms).

Table I lists the cross section peak integrals I_c as well as the centroid energies E_c and the widths σ_c (in MeV) as discussed above and used for the approximate considerations presented in sections IX to XI. In Figs. 7 to 25 the corresponding results are shown as blue lines. The relative importance of the components listed is not easy to visualize for the many nuclei under study here, as there are considerable variations with A and Z . As will be shown in the next section the level density increases strongly when approaching S_n and due to the convolution with the photon strength function the sensitivity of radiative capture peaks at $E_x \approx 3-5$ MeV [sc11] – far below S_n . Clearly the main contribution to this process is due to the electric isovector dipole mode described by TLO. The other important contributions to the photon strength are related to the pigmy resonance and to the orbital magnetic “scissors” mode [he10], at least in nuclei with sufficiently large β . The spin flip M1 strength values listed in the Table are upper limits deduced from experimental information [la87, sc07, he10]; this mode with its elevated energy has a reduced influence on radiative neutron capture. Contrariwise the electric dipole strength due to the phonon coupling of the type $(2^+ \times 3^-)_{1^-}$ is of some importance, but is difficult to quantify in a scheme which is applicable to the full range of nuclides in question, and thus respective predictions clearly have an uncertainty. It also is mentioned, that for transitions between two high lying levels E1, M1 and E2 transitions may be important that are not accessible by studies with photon or electron beams.

IX Level densities

Intrinsic state density

Nuclear level densities $\rho(E_x, J^\pi)$ determine the final phase space for predictions of compound

nuclear cross sections and decay rates. In a compilation [ca09] of data extracted from nuclear spectra and neutron capture resonance spacings it was shown that when they are parameterized in various ways, this may lead to inconsistent predictions. Hence the need of calculations based on fundamental principles, which rely on very few free parameters only, is indicated. A clear distinction has also to be made between the intrinsic quasiparticle state $\omega_{qp}(E_x)$ and the level density $\rho(E_x, J)$ in the observer's system. Here an analytical approach is used for the calculation of ω_{qp} on an absolute scale and avoid as far as possible parameter adjustments by strongly relying on statistical laws for a Fermi gas – here a system of independent spin $\frac{1}{2}$ -particles with some mean attraction. As shown [er60] it is characterized by a gap $\Delta(t)$ falling with rising temperature parameter t down to 0 at a ‘critical’ $t_{pt} = \Delta_0 \cdot e^C / \pi = 0.567 \cdot \Delta_0$ (with the Euler constant $C=0.5772$), indicating a phase transition [la64, gr85, mo15], governed by pairing. It was shown [gr85] that in infinite nuclear matter (nm) the backshift energy E_{bs} , which describes a backshift between the Fermi gas zero and the nuclear matter ground state, is equal to the pairing condensation energy E_{con} , described below by Eq. (22). Canonical thermodynamics has been used for nuclear matter to evaluate the general features of this phase transition, and all effects appearing in finite nuclei can be treated micro-canonically [gr85]. Following earlier work [gi65] and a recent data analysis [mo15, gu15], the energy dependence of the state density is assumed to be exponential for lower energies, *i.e.* in the pairing dominated phase below the phase transition point. If only quasiparticle excitations are considered the total state density (in the intrinsic frame) $\omega_{qp}(E_x)$ at excitation energy E_x is then approximated by:

$$\omega_{qp}(E_x) = \omega_{qp}(0) \exp\left(\frac{E_x}{T_{ct}}\right) \text{ for } E_x < E_{pt} \quad (19)$$

$$\omega_{qp}(E_x) = \frac{\exp(2\sqrt{\tilde{a}(E_x - E_{bs})})}{\frac{12}{\sqrt{\pi}} \tilde{a}^{1/4} (E_x - E_{bs})^{5/4}} \text{ for } E_x \geq E_{pt} \quad (20)$$

For the Fermi gas phase of infinite nuclear matter (nm) the ‘level density parameter’ a_{nm} is required to be inversely proportional to the Fermi energy ε_F as was demonstrated [bo75]. It also determines the energy E_{con} of the pairing induced condensation [gr85, ig93, ca09, ko08, eg09]. At the phase transition (corresponding to t_{pt}) the excitation energy is $E_{pt} = a_{nm} \cdot t_{pt}^2 + E_{bs}$ and a transition from a Fermi gas like behaviour above to a pairing dominated regime below the transition point occurs. The latter region is approximated by the assumption of constant temperature and it will be discussed below, how the phenomenological parameters T_{ct} and $\omega_{qp}(0)$ are determined in heavier nuclei for this low energy region.

In the Fermionic regime ($E \geq E_{pt}$) of finite nuclei, the backshift E_{bs} stands for the energy between the Fermi gas zero and the nuclear ground state as in nuclear matter, but it has to be corrected for shell effects. To obtain a level density parameter \tilde{a} for a given A a surface addition term δa to a_{nm} is introduced, quantified by α ; α is found to be as small as $\alpha = 0.06$, when treated as a global parameter – actually the only one in the present fit to neutron capture resonance separation data:

$$a_{nm} = \frac{\pi^2 A}{4\varepsilon_F} \approx \frac{A}{15}; \quad \tilde{a} = a_{nm} + \delta a; \quad \delta a = \alpha \cdot A^{2/3} \quad (21)$$

$$E_{con} = \frac{3}{2\pi^2} a_{nm} \Delta_0^2; \quad E_{bs} = E_{con} - \delta E(Z, A) \quad \text{and} \quad E_{pt} = \tilde{a} \cdot t_{pt}^2 + E_{bs} \quad (22)$$

As pointed out [gr14], various approximations are required and listed here albeit not all of them are of significant influence for the conclusions made in this work:

1. The pairing parameter $\Delta(E_x=0)$ is approximated by $\Delta_0=12\cdot A^{-1/2}$, independent of angular momentum.
2. Δ_0 is used for neutrons and protons and thus independent of neutron excess $N-Z$.
3. Quasi-particle states are evenly spaced (at least on average) at the Fermi energy, not varying with $N-Z$.
4. Fermi energy $\varepsilon_F = 37$ MeV and nuclear radius $R = 1.16\cdot A^{1/3}$ are independent of $N-Z$; they control a_{nm} for nuclear matter and the phase transition [la64, gr85] at excitation energy E_{pt} .
5. A dependence of equilibrium deformation on excitation energy E_x and angular momentum J is neglected beyond its implicit influence via $\delta E(Z,A)$ in Eq. (22).
6. A factor 1/4 accounts for \mathcal{R}_π -invariance [bj74].
7. The moments of inertia, which will be shown to have nearly no effect at low spin, are taken from a rigid rotor.
8. The influence of shell effects is controlled by $\delta E(Z,A)$, extracted by subtraction of the experimental mass from liquid drop values, following ref. [pe01].
9. At variance to previous work [ig93, ca09, ko08, eg09, me94] the shell correction term is directly applied to the backshift energy E_{bs} [gi65, ka78, ju98]. No dependence on deformation is included.

It was shown [gr85] that the expression given by Eq. (20) for ω_{qp} in the Fermi gas regime – initially derived neglecting pairing [bo75, gi65] – is a good approximation for the formalism derived with a thorough (micro-canonical) inclusion of pairing, if E_x is back-shifted by the condensation energy E_{con} , which already appears in infinite Fermionic systems and which is independent of A . In finite nuclei the back-shift E_{bs} as given in Eq. (22) combines this pairing term with the effective shell correction $\delta E(Z,A)$ which includes the odd-even mass difference. The intrinsic (quasi-particle) state density $\omega_{qp}(E_x)$ for the Fermionic region as well as for E_{pt} are given by Eqs. (20 to 22). Below E_{pt} an interpolation of $\omega_{qp}(E_x)$ to the ground state is found by Eq. (20); the simple approach of a logarithmic interpolation in analogy with an exponential increase of $\omega_{qp}(E_x)$ has been shown to be a reasonable approximation to the low excitation structure of heavy nuclei [gi65, ko08, ca09, mo15, gu15]. At variance to that work E_{pt} is fixed using \tilde{a} , t_{pt} and E_{bs} and the requirement of a continuous transition in $\omega_{qp}(E_x)$ at E_{pt} to determine T_{ct} .

In principle $\omega_{qp}(0)$ can be fixed locally by regarding known spectral data ($E_x < \Delta_0, J$), similar as has been done previously [sc11, ru13, ma12]. When $\omega_{qp}(0)$ is globally approximated by $0.3/\Delta_0$ for the state density at the lower end of the interpolation just above ground. This is a first approximation only and it will be discussed below that there is some effect on the predictions for average radiative widths and neutron capture cross sections. From Eq. (20) one sees, that a temperature parameter, defined like for a Fermi-gas at the saddle point by an approximation [gi65, bo75, gr85] of the Laplace transform, $t = \sqrt{(E_x - E_{bs})/\tilde{a}}$ differs from an apparent nuclear temperature $T_{app} = \frac{\omega}{\partial\omega/\partial E}$. It appears that also T_{ct} is smaller than T_{app} by up

to 35% and this results in a sudden change in the slope of $\omega(E_x)$ at E_{pt} (cf. Fig. 28). Close to magic nuclei the large (negative) shell correction results in such a break at the now large E_{pt} , but for weakly bound nuclei (e.g. near the edge of stability) E_{pt} becomes small and the Fermi gas phase starts already at low E_x . It can be seen in Fig. 27, that for more than 100 of the 146 nuclei investigated here E_{pt} is smaller than S_n and thus the neutron capture resonances fall into the Fermi gas regime, but the subsequent gamma decay preferentially ends below E_{pt} and the level density there is important for the prediction of radiative capture cross sections. The Figure also shows that in the Eq. (22) E_{pt} and δE are symmetric against E_{con} , which is independent of A . It also becomes obvious, that in the Fermi gas regime $\delta E(Z,A)$ is closely correlated to E_{pt} and thus also to $\omega_{\text{qp}}(E_x)$; it is hence the quantity of importance for a level density prediction and S_n plays a minor role, at variance to a previous assumption [gi65]. It is remarkable that in some weakly bound nuclei the phase transition is predicted to already occur below $E_x = 3$ MeV

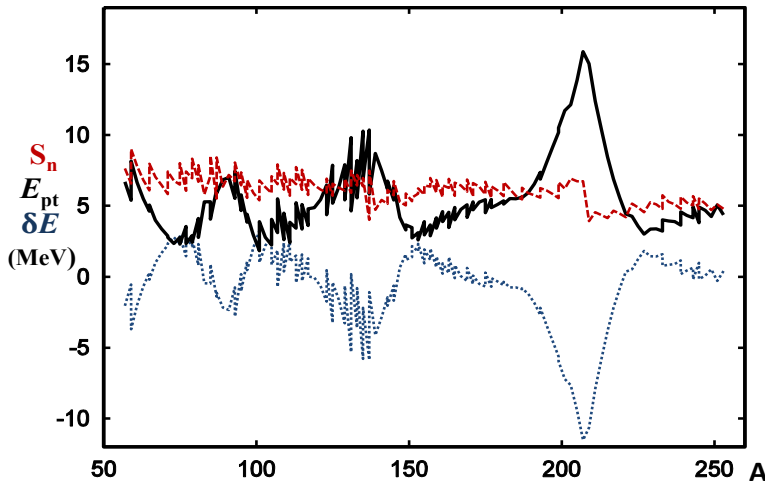


Fig 27: Phase transition energy E_{pt} for nuclei in the valley of stability vs. A (full line in black) in comparison to values for S_n (dashed in red) and the shell correction energy δE_x (blue dots) all in MeV.

The quantities to be compared to observed level spacings have to be derived from $\omega_{\text{qp}}(E_x)$ by a projection on angular momentum J in the observer system. The proposal was made [bo75, gi65, hu74, vi82] to consider the M-substate distribution of $\omega_{\text{qp}}(E_x)$ as Gaussian with width σ around $M = 0$ and to differentiate at $M = J+1/2$ with respect to M . This leads to a spin dependent level density [bj74, bo75, gr85, ig93, mu98, eg09, ko08, ca09]:

$$\rho_{\text{sph}}(E_x, J) \cong \frac{2J+1}{\sqrt{8\pi} \sigma^3} e^{-\frac{(J+1/2)^2}{2\sigma^2}} \omega_{\text{qp}}(E_x) \xrightarrow{\text{small } J} \frac{2J+1}{\sqrt{8\pi} \sigma^3} \omega_{\text{qp}}(E_x) \text{ with } \sigma = \sqrt{\frac{\Im \cdot t}{\hbar^2}} \quad (23).$$

The spin dispersion σ depends on the nucleus' moment of inertia \Im , often assumed to be the rigid rotor value [bo75]. The redistribution of the quasi-particle states into levels of distinct spin as incorporated here implicitly assumes [vi82] the nucleus to be exactly spherical symmetric even at $E_x \cong S_n$. This neglects strongly mixed modes which, due to their collectivity, are pulled from their original quasi-particle energy down into the low excitation region. Without assuring spherical symmetry for the nuclei studied, Eq. (23) has found a widespread use [gi65, ka78, gr85, ig93, me94, eg09, ca09]. In some work the rotational collectivity present in an axially symmetric nucleus was included at this stage as extra term [bo75, bj74, hu74, vi82, ju98], yielding a level density enlargement by a factor σ^2 (i.e. $\approx A/5$)

as compared to Eq. (23). But still an agreement with observations was not reached without a significant enlargement of \tilde{a} as compared to a_{nm} [hu74, bo75, ca09, ma12].

Collective enhancement

It will become obvious that the absolute scale of any prediction for the level density is strongly influenced by allowing for broken axial shape symmetry in the Fermi gas regime and at E_{pt} . In previous work [ca09] deficits in the comparison to resonance spacings observed at the neutron binding energy S_n have been compensated by an increase of the level density parameter \tilde{a} , eventually adjusted in a fit. But an agreement to observations was not reached without a significant enlargement of \tilde{a} as compared to a_{nm} as demonstrated [ca09]. In addition an excitation energy dependence of ρ was introduced - at variance to the Fermi gas, which can well be accepted as proper description of the statistics in highly excited nuclei. For a comparison to experimental data such a modification is not needed as a significant collective enhancement of ρ results from not using the scheme presented for the case of spherical or axial symmetry [er60]. An inclusion of the effect from missing axial symmetry follows a proposal made long ago [bj74], but not taken up by subsequent studies. With a factor 1/8 for \mathcal{R}_π -invariance and parity conservation one obtains from this for the density of levels with both parities, which results in an astonishingly simple expression for small J – as already presented by Bohr and Mottelson [bo75], *cf.* Eq. (4-65b):

$$\rho(E_x, J^\pi) \cong \frac{\sqrt{8\pi}}{8} \cdot \frac{\sigma_1 \sigma_2 \sigma_3}{\sigma^3} \cdot \frac{2J+1}{\sqrt{8\pi}} e^{-\sum_i \frac{(J+\frac{1}{2})^2}{2\sigma_i^2}} \omega_{qp}(E_x) \xrightarrow{\text{small } J} \frac{2J+1}{8} \omega_{qp}(E_x) \quad (24)$$

In view of the IVGDR splitting observed in nearly all nuclei with $A > 50$ – as described above – it is important to account for the enhancement of level densities resulting from the build-up of a rotational band on each intrinsic quasi-particle state: *The total level spectrum, for a given angular momentum, is therefore obtained by summing over a set of intrinsic states rather than by a decomposition of the level spectrum, as for a spherical system* [bj74]. For an equilibrium shape that possesses all the rotational degrees of freedom of a three-dimensional body and thus completely violates rotational symmetry, in the sense that it is not invariant with respect to any rotation of the coordinate axes, such a rotational band on top of every intrinsic state involves $(2J+1)$ levels with total angular momentum J . Each of these levels is itself $(2J+1)$ -fold degenerate, corresponding to the different components M [bj74]. The rotation induced collective enhancement may fade out at higher energy, but this will happen only far above the energy range around S_n , of interest here [ha83, ju98, gr11]. As usual [er60, gi65, bo75], it is assumed in Eq. (24) that the excitation energy E_x is large as compared to the rotational energy $\frac{\hbar^2 J(J+1)}{2 \cdot \mathfrak{J}_k}$ and that the spin projections m are normally distributed around 0. The moments of inertia \mathfrak{J}_k describe a collective rotation with respect to the axis k , and \mathfrak{J}_s refers to the statistical quasi-particle motion, responsible for the spin dispersion $\sigma^2 = \mathfrak{J}_s \cdot t \cdot \hbar^{-2}$. The proposition made [bj74, bo75] to identify σ with the smallest \mathfrak{J}_k and thus with the smallest spin cut off factor σ_i is modified here by setting $R_\sigma = \sigma_1 \cdot \sigma_2 \cdot \sigma_3 / \sigma^3 \equiv 1$; it is also assumed, that the exponential spin cut off factor can be neglected in the limit for small J . The reduction by 4 is related to the invariance with respect to rotations by 180° about each of the three principal axes, valid for the most general quadrupole deformation [bj74, bo75]. If the nuclear body is completely symmetric about one axis, i.e. axially deformed, an additional decrease of the

level density by $\sqrt{\pi/2} \cdot \sigma \cong 8$ is expected in the limit of small J , and a reduction by ≈ 300 – from $\sqrt{\pi/2} \cdot \sigma^3$ – has to be included in Eq. (23) for the level density of completely spherical nuclei [er60, bj74, bo75]. The size of these factors indicates that the dependence of the absolute level density on the symmetry of the nuclei is appreciable, whereas the size of the deformation enters only via σ and also σ_i . As the deformation parameters β and γ are subject to fluctuations around their mean values [de10] a shape sampling equivalent to the one described for the axis lengths was applied to the moments of inertia. Such sampling does not affect the symmetry class and its effect on R_σ and thus on $\rho(E, J^\pi)$ was found to be negligible by respective calculations. Low energy oscillations in heavy nuclei have been assumed to lead to vibrational bands and to cause another [bj74, ju98] collective enhancement of $\rho(E, J^\pi)$. In this scheme the extra level density is accounted for by the breaking of axial symmetry; the effect of low energy quadrupole vibrations was investigated in analogy to the isoscalar quadrupole giant resonance (ISGQR) by inserting $\hbar\omega_{\text{vib}} = \frac{1}{3} E_{\text{ISGQR}}(2^+)$ and $I_{\text{vib}} = \frac{1}{8} I_{\text{ISGQR}}(2^+)$ in the expression for the strength functions as compiled in Table I.

Comparison to data

Average level distances $D_{\text{int}}(E, J^\pi)$ are available from ensembles of discrete levels with equal spin populated in nuclear reactions at low E_x and at the neutron separation energy S_n from compound resonances in the cross section for neutron capture in the eV and keV range. For a test of the outlined formalism for odd- n nuclei with a satisfactory number of levels were selected from a comprehensive data compilation [ca09]. The experimental information on $\rho(Z, N, E_x, J^\pi)$ stems from counting bound levels up to an E_x , above which completeness is no longer assured, as well as resonances just above S_n [ko08, ca09]. As their spins are known, only 3 obvious assumptions are needed to obtain $\omega_{\text{qp}}(E_x)$ from the data by using Eq. (24):

1. Parities are equally distributed in the discrete spectrum;
2. The bracket containing the spin dispersion factor has the value $R_\sigma = 1$;
3. σ_s in the exponential spin cut-off correction is taken from systematics [eg09].

This procedure of applying the spin dependent factors to the data allows different spins to be shown in the same plot. To demonstrate the energy dependence of the level density formalism presented here, results for ^{81}Sr , ^{113}Cd and ^{235}U are given in Fig. 28.

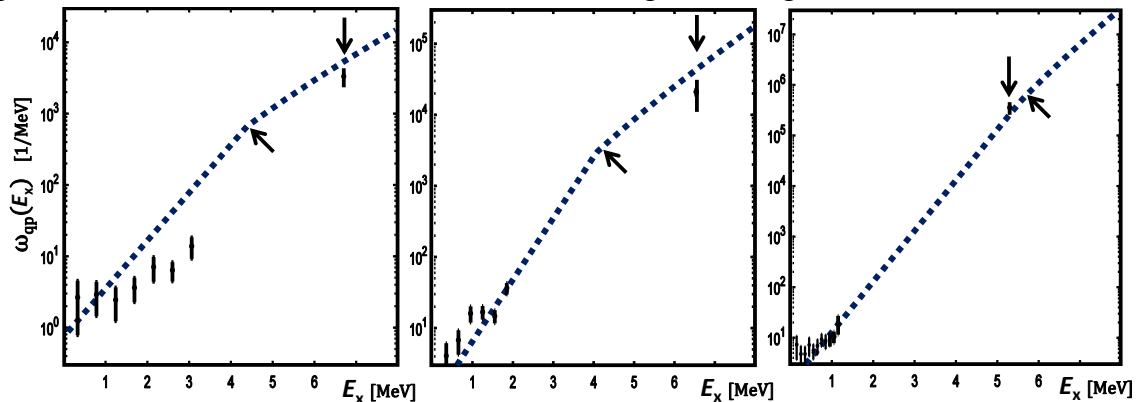


Figure 28. For the state density $\omega_{\text{qp}}(E_x)$ in the nuclei ^{81}Sr , ^{113}Cd , and ^{235}U the prediction is shown together with respective data from Ripl-3 [ca09] obtained using discrete levels (black \blacksquare) [ig06, ca09] as well as resonance spacings (below vertical arrow); both are converted into state density ω by inverting Eq. (24). A change in slope at the phase transition energy E_{pt} is clearly seen (diagonal arrow). The dotted line in blue depicts Eqs. (20 to 22).

As will be shown in section X, the slope below S_n is of special interest for capture cross sections. It is reasonably well predicted even for ^{81}Se , although some data are missed in absolute height by approximately the factor introduced above for axially symmetric shapes. Extrapolations into domains away from stability need global parameterizations valid for an extended region of nuclei. For 132 nuclei with $A > 70$ the average distance of s-wave neutron capture resonances is available [ig06]. As these all have spin $\frac{1}{2}^+$, it is interesting to compare these data to Eq. (20), which represents the most general, triaxial case. It is worthwhile noting that for spin $\frac{1}{2}$ the small J limit is lower by a few % only.

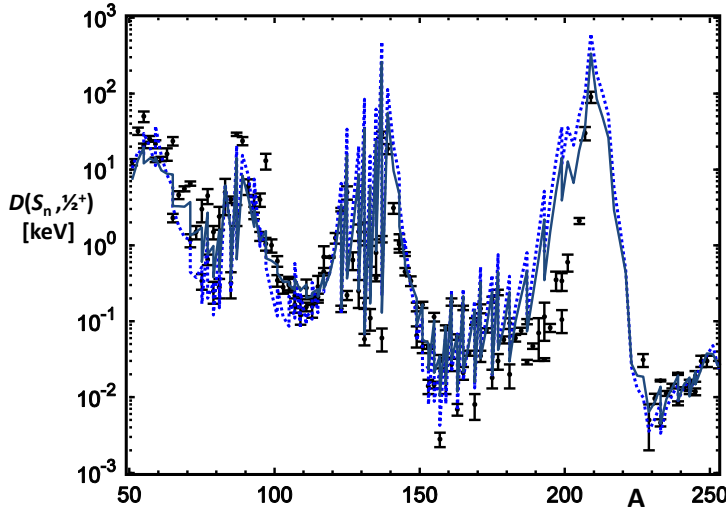


Fig. 29: Average resonance spacings $D(S_n, \frac{1}{2}^+)$ in nuclei with $51 < A < 253$ as observed in neutron capture by spin 0 target nuclei. Data (I) compiled by the RIPL collaboration [ig06, ca09] are compared to the prediction with an effective shell correction [pe01] as presented in section IX (dots). The drawn line depicts the case when it is damped with E_x as proposed previously [ka78].

Fig. 29 depicts the results from using Eqs. (20 to 22 and 24) to measurements available for 132 nuclei and apparently many of the lie close to the prediction. The shell correction plays an important for the resulting agreement; it is improved by including a damping of as proposed previously [ka78]. This accord over many orders of magnitude is reached with the only fit parameter $\alpha = 0.06$, It is of interest to find out, if alternatives proposed earlier change the situation and eventually indicate a way to obtain an even better global fit. The reduction of the nucleon mass to an effective in-medium value was suggested [mu98], deviations of nuclear radii from $1.2 \cdot A^{\frac{1}{3}}$ fm are documented [de10], model calculations of moments of inertia show considerable differences to rigid rotor values [po73], and ambiguities may be seen in the choice of temperature (T vs. t). Because of a cancellation in R_σ these topics do not change the collective enhancement given by Eq. (24) and their influence only leads to a small and insignificant change of the prediction. An important influence on the intrinsic state density $\omega_{qp}(E_x)$ as well as on $\rho(E_x, J)$ was found to emerge from the choice made for dE , by which the Fermi gas zero is fixed with respect to the nucleus' ground state: Replacing the liquid drop model masses from ref. [my67] by the one from [me94] increases the level density for actinide nuclei by nearly an order of magnitude, whereas the use of ref. [mo95] has the opposite effect. The recent liquid drop model fit to masses [pe01] used in this study is based on fitting a volume and a surface term independently and the resulting accord to resonance

spacings are shown in Fig. 29. A nearly equally good agreement is found for the choice [my67] made recently [gr14], but a new LDM fit including a curvature term leads to a significant over-prediction for actinide nuclei. Unfortunately these LDM fits are made neglecting the breaking of axial symmetry, as its influence on ground state masses was calculated to be very small for most heavy nuclei [mo95, mo06]. Hence more theoretical studies on the A-dependence of dE seem indicated; a broad mass range should be regarded, as a large effect of the LDM fits to dE is seen for $A \approx 60$ and $A \geq 230$, but only small differences between various LDM for $A \approx 80$ to 140. The agreement to experimental level densities resulting from the used LDM fit [pe01] may well be regarded as an additional indicator for its quality, as it also supports the parameterization presented here.

X. Radiative neutron capture

General remarks

The radiative capture of fast neutrons by heavier nuclei plays an important role in considerations for advanced nuclear systems [ro57, ch06] and devices aiming for the transmutation of radioactive nuclear waste. This process is of interest also for the cosmic nucleosynthesis, especially for scenarios with such high neutron flux, that neutron capture processes can be the cause for a production of nuclides beyond Fe [bu57, ka89]. To test the combination of the present ansatz on the photon strength to the one for the level density – both allowing for a breaking of axial symmetry – a comparison on absolute scale of predicted to measured average radiative widths is demonstrated first. A sum over the decay channels to all bound states J_b which can be reached from the capture resonances J_r by dipole photons of energy $E_\gamma = E_r - E_b$, multiplied by their density $\rho(E_b, J_b)$ leads to an effective averaging. The dependence of $\rho(E_b, J_b)$ on J_b (cf. Eq. (24)) has the consequence that the γ -decay for dipole-transitions from $J_r = 1/2$ to $J_b = 3/2$ is favoured as compared to final levels with $J_b = 1/2$ and a difference between E1 and M1 arises, if there is a parity dependence of the level density. In the ansatz discussed here, $\rho(E_x, J)$ above E_{pt} is determined by the Fermi gas prescription and independent of parity by principle. One may account for differences in the low energy regime caused by a dominant parity through a respective estimate of $\omega(0) \equiv \omega(E_x < \Delta_0)$, if respective information is available; this may improve the predictions. The mean radiative width in $J_r^\pi = 1/2^+$ of final isotopes is the basis for the description of radiative capture by 0^+ -target nuclei with $\ell_n = 0$ as discussed in the following.

Average radiative widths

It was pointed out previously [ko90] that strength information can be extracted from capture data directly by regarding average photon widths $\bar{\Gamma}_\gamma$. These are proportional to the ratio between the level densities at the capturing resonances r – included in $f_1(E_\gamma)$, as shown in Eq. (14) – and at the final states b below S_n reached by $E_\gamma = E_r - E_b$, and depend in addition on the photon strength, *i.e.* the low energy tail eventually extrapolated from above. It is known that $\bar{\Gamma}_\gamma$ does not vary with E_r [la57, ba73] and hence it can be approximated for $J_r = 1/2^+$ by setting $\lambda = 1$ in Eq. (14) and summing over all final bound levels $b \in \Delta_b$, *i.e.* over $\Delta_b = [0, S_n + E_r]$:

$$\bar{\Gamma}_\gamma = \sum_{b \in \Delta_b} \Gamma_\gamma(r \rightarrow b) \cong \rho(E_b, J_b) \cdot \langle \Gamma_\gamma(r \rightarrow b) \rangle \cdot \Delta_b \cong \int_{\Delta_b} \frac{\rho(E_b, J_b)}{\rho(E_r, J_r)} f_1(E_\gamma) E_\gamma^3 dE_\gamma \quad (25).$$

One sees, that the average radiative widths vary with the slope of $\rho(E_x, J)$ in the range from E_b to E_r , in contrast to capture cross sections which also vary with the level density at S_n [gi65, eg09, ca09]. Average radiative widths were derived by a resonance analysis of neutron data taken just above S_n and tabulated [ig06] for 115 even-odd nuclei with $51 \leq A \leq 253$. These $\langle \Gamma_\gamma \rangle$ allow a combined test of predictions for photon strength and level densities, and respective data are shown in Fig. 30. Radiative capture into spin-0 targets only through the s-channel ($\ell_n=0$) is considered, such that the spin dependence of the level densities $\rho(E_r, J_r)$, under dispute recently [eg09], can be neglected and the spin cut off in Eq. (24) is neglected here assuming, that the collective energy to be added to the intrinsic excitation is small as compared to E_γ . Magnetic (M1) strength was treated separately and then the number of levels with $J^\pi = \frac{1}{2}^+$ and $\frac{3}{2}^+$ at low energy enters explicitly. They play a minor role for the energy integrated photon interaction, as resulted from inserting tabulated [ra01, ca09] values for the matrix elements and recent experimental data [ju08, sa13, ma14]. It appears that, similar to non-nuclear systems, electric dipole modes dominate radiative processes.

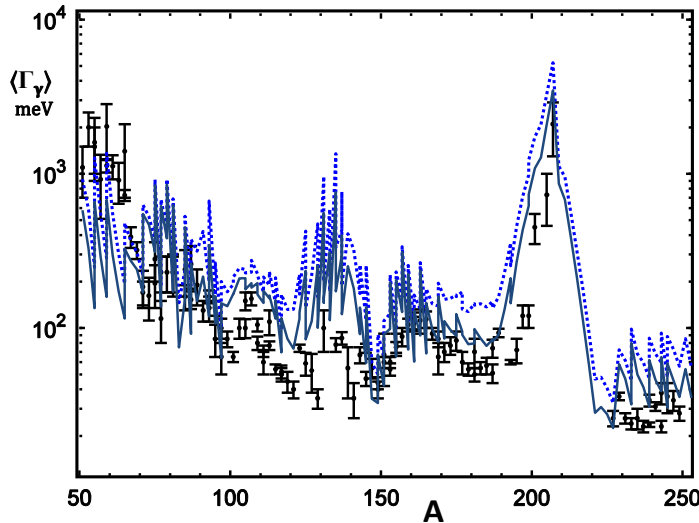


Fig. 30: Average radiative widths as determined experimentally for nuclei populated by radiative neutron capture by spin 0 targets with $A > 50$ shown in black [ig06] are compared to calculations. The combination of the complete dipole strength described in sections V to VIII with the level density as given in section IX is depicted as drawn line and the dots indicate an increase of $\omega_{qp}(0)$ by 3.

As shown in Fig. 30, the agreement between prediction and data is satisfactory and again this can be attributed to the introduction of a LDM based shell correction. There are local discrepancies – especially just below ^{208}Pb – probably related to the neglect of shell effects (other than $\delta E(Z, A)$) in the proposed ansatz for the level density and the apparent disagreement for $A < 70$ may have a similar origin. The comparison to existing experimental data for $\langle \Gamma_\gamma \rangle$ as depicted in Fig. 30 uses the photon strength as discussed in sections VI to VIII and the level density obtained from the parameterization described in section IX. This is at variance to previous work which only covered limited numbers of nuclides and used parameters for $\rho(E_x)$ locally adjusted to low lying levels and neutron resonances [ko90, be95, ut08, ut11, la10]. The good accordance to experimental data on absolute scale as shown in Fig. 30 enables an evaluation of the importance of various approximations applied: A decrease of $\omega_{qp}(0)$ by a factor of 3 modifies $\langle \Gamma_\gamma \rangle$ by 20 to 50 % when regarding nuclei with A

≈ 70 resp. $A \approx 240$ and this shows that the agreement may be improved by an introduction of local spectroscopic information, not included in this parameterization, explicitly based on global properties only. The inclusion of all the various components of minor strength as listed in Table I increases $\langle \Gamma_\gamma \rangle$ by $\approx 55\%$ for an average over A . The largest effect (nearly 40 %) was found for the coupled mode $(2^+*3^-)_{1^-}$, studied theoretically [bo57] since long, but for its strength only data scattered in A and Z are available [kn06], which were used as guide here. The second largest increase of $\langle \Gamma_\gamma \rangle$ (by $\approx 10\%$) is due to magnetic dipole strength and a low-energy E2 component of strength as given and discussed with Table I was found to increase a decay of the $\frac{1}{2}^+$ -levels just above S_n , as populated via s-capture, by less than 7 % albeit the opening of E2-decay to $\frac{5}{2}^+$ levels. On average over A , an increase of $\langle \Gamma_\gamma \rangle$ due to the inclusion of pygmy strength as discussed stays below 5%.

Averaged cross sections for radiative capture

As known from measured neutron strengths as listed for RIPL-3 [ig06, ca09] the neutron widths above ≈ 1 keV are that large, that $\langle \Gamma_n \rangle \gg \bar{\Gamma}_\gamma$ and the average over the width ratio can be replaced by $\bar{\Gamma}_\gamma$ with an accuracy of a few percent. This is done in Eq. (26a), where use of optical potentials for the compound nucleus formation and a fully statistical treatment of its decay are replaced by a schematic ansatz [la57].:

$$\langle \sigma(n, \gamma) \rangle_r \cong 2\pi^2 \lambda_n^2 \cdot \sum_{\ell} (2\ell_n + 1) \cdot \left\langle \frac{\Gamma_n \cdot \bar{\Gamma}_\gamma}{\Gamma_n + \bar{\Gamma}_\gamma} \right\rangle_r \cdot \rho(E_r, J_r) \quad \text{with} \quad \left\langle \frac{\Gamma_n \cdot \bar{\Gamma}_\gamma}{\Gamma_n + \bar{\Gamma}_\gamma} \right\rangle_r \cong \bar{\Gamma}_\gamma \quad (26a).$$

As $\bar{\Gamma}_\gamma$ is contained implicitly in $f_1(E_\gamma)$ one gets from Eq. (25) $\sigma_c(E_n)$ for $E_n = E_r - S_n$:

$$\sigma_c(E_n) \equiv \langle \sigma(n, \gamma) \rangle_r \cong 2\pi^2 \lambda_n^2 \cdot \sum_{J_b} (2\ell_n + 1) \cdot \int_0^{E_r} f_1(E_\gamma) E_\gamma^3 \cdot \rho(E_b, J_b) dE_\gamma \quad (26b).$$

It shows that the neutron energy enters mainly via λ_n in this cross section formula for $\sigma_c(E_n)$ and, following theory [la57], one arrives at Eq. (27) for the Maxwellian averaged radiative capture cross section (MACS). Problems related to non-zero target spins in radiative capture averaged over many resonances need additional work as well as the neglect of $\ell > 0$, direct capture and inelastic scattering. A prediction of MACS based on the photon strength presented in sections VI to VIII is then possible, when calculated by:

$$\langle \sigma(n, \gamma) \rangle_{kT} \cong \frac{2}{\sqrt{\pi}} \frac{\int_0^\infty \sigma_c(E_n) E_n \cdot e^{-E_n/kT} dE_n}{\int_0^\infty E_n \cdot e^{-E_n/kT} dE_n} \quad (27).$$

As pointed out [ka11], the folding of experimental cross sections as well as those given by Eq. (26) with a Maxwellian distribution of neutron energies is straightforward. In view of the fact that $D \gg \Gamma_r \gtrsim \Gamma_{r\gamma}$ the Maxwellian averages around 30 keV are formed incoherently with neglect of Porter-Thomas fluctuations. By only regarding the radiative capture by spin-zero targets effects related to ambiguities of spin cut off or dispersion parameters and angular momentum coupling are suppressed, but still the data vary by about 4 orders of magnitude in the discussed range of A – and are well represented by the TLO-parameterization used here together with the proposed ansatz for $\rho(A, J^\pi, E_x)$, as is obvious from Fig. 31.

The overall agreement on absolute scale and over more than three decades is remarkable; a

discrepancy observed in the region of $A > 230$ may well be related to an over-prediction low energy components in state density or strength function, which have strong important in the high mass range. This and other local effects originating from details of the shell structure cannot all be treated in this review, the main topic of which – the importance of triaxiality in heavy nuclei – is not influenced significantly by discrepancies of this small size.

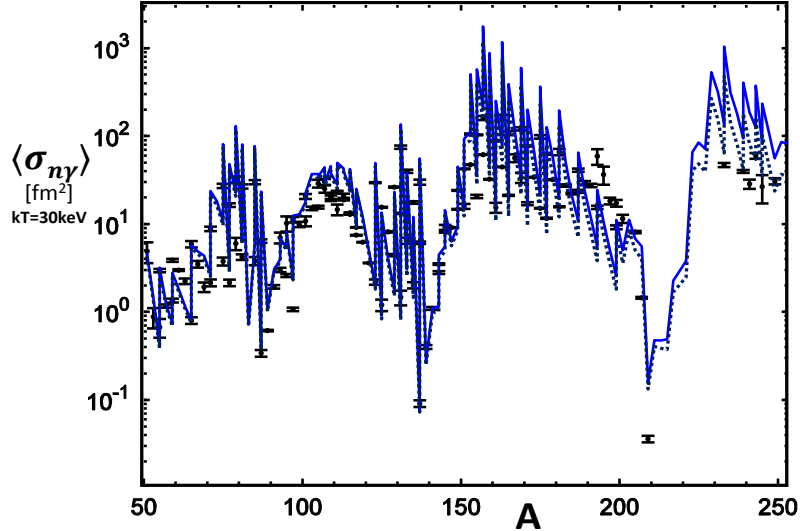


Fig. 31: Maxwellian averages of measured cross sections for radiative neutron capture into even nuclei with $J=0$ and $50 < A < 250$ ($\text{+}, [\text{di10, pr10}]$) for $kT_{AGB} = 30$ keV. They are plotted vs. A_{CN} in comparison to calculations based on Eq.27 with TLO (dotted line) and including the minor components listed in Table I (full line). The level densities are determined as described in section IX.

As already mentioned before [sc10] and in section VII the impact of photon strength on radiative neutron capture cross sections is peaking in the region below $E_\gamma \cong 6$ MeV. Below, the factor $E_\gamma^{2\lambda+1}$ reduces the transition rates and above the density of levels to be reached becomes small. Thus the scissors mode, which is prominent in deformed nuclei, has the strongest effect on M^1 -transitions, and the non-IVGDR ‘pigmy’ E1-strength has to be regarded as well. As depicted in Fig. 31 by the dashed curve the cross section is dominated by the IVGDR extension. Recent works on the influence of minor strength components indicate a more significant impact in comparison to the IVGDR tail [gy98, li09, la10]. This may be appropriate for very neutron rich nuclei with their small S_n , but not in the valley of stability; it was shown in section VII, that single or double Lorentzians result in erroneous estimates of the corresponding E1-strength in the tail. This is especially so if a dependence of Γ_γ on E_γ is imposed [ka83, ko90] to seemingly improve the fit of the IVGDR. Namely the gamma-energy dependence of the resonance widths imposed there plays an important role. In the TLO approach the sole variation of Γ with the pole energy, its global adjustment and the strict implementation of the TRK sum rule avoid irregularities of the dipole strength prediction for the tail region below the IVGDR.

Fast neutron induced transmutation

One – for many even the strongest – of the arguments against a long-lasting commitment to nuclear power as energy supply is the difficult permanent disposal of the long lived radioactive waste produced in nuclear reactors. Significant efforts are thus being made

worldwide directed towards the minimization, management, and disposal of highly radioactive nuclear waste. Thus the partitioning of nuclear waste and transmutation of long-lived isotopes to nuclides with shorter lifetime are being investigated worldwide. Different schemes have been proposed that may reduce the radioactivity and radio-toxicity of the spent fuel after burn up. The studies towards the choice of the best options make extensive use of simulation methods in order to predict the system behaviour in a great variety of possible configurations and running conditions [sa11]. A fundamental prerequisite for these computations is the availability of reliable cross section data. These are needed for processes and operating parameters that are significantly different from those of current systems mostly operating with thermal neutrons. A good understanding of the radiative capture of fast neutrons is an important part for any theoretical attempt in this direction, and the agreement shown in Fig.31 appears promising.

But a much more severe problem with nuclear reactor waste is posed by the presence of nuclides beyond ^{238}U produced in the high flux of slow neutrons in the ^{238}U usually forming a large fraction of the fuel. By multiple neutron capture and subsequent β -decay an appreciable amount of long lived nuclides are formed. As several of these “minor actinides” are α -emitters the risk of their incorporation increases their high radio-toxicity. Attempts to expand the TLO-based calculations of (n,γ) cross sections to actinide nuclei are hampered by serious discrepancies between IVGDR data observed in different laboratories, some of which are obvious from the figures shown. As neutron capture by actinide nuclei is of great importance for the transmutation of nuclear waste the special investigation of neutron capture cross sections for Th, U and heavier nuclei, for which data were compiled [pr10], is useful. The fact, that TLO results in a good description of the data for ^{239}Pu (cf. Fig. 25) and the good match observed in Fig. 31 leads to consider the TLO approach as encouraging to serve as guideline for predictions concerning the radiative capture of fast neutrons also for actinide nuclei. Whereas the approximations made to arrive at Eq. (26) work well in the range of $E_n \approx 30$ keV (see Fig. 31) the coupling to other channels like inelastic scattering has to be included at higher energies. The effect of further contributions was shown recently in detail for ^{238}U [ul87] and for other actinides [gu12], where also the importance of the scissors mode was pointed out. In view of the average overall agreement for more than 150 nuclides as presented in the previous section to experimental (γ,n) -averages an inclusion of the TLO dipole strength and the ‘triaxial’ level density as an option in TALYS [ko08] or EMPIRE [he07] appear highly desirable. The two codes named here – as well as others – use the “old” Lorentzian descriptions [ko90, ca09] of the IVGDR shapes with only one or two poles and locally adjusted IVGDR parameters.

Also the neutron energy dependence of the measured $\sigma(n,\gamma)$ is quite well reproduced in the region around 30 keV [gr11] by the prediction of Eqs. (26) and (27). The agreement found for these actinide nuclei is similar to the one seen in Fig. 31, although the reaction dynamics as the coupling between different channels – important for higher neutron energies [la57] – are not implicitly accounted for. Of course, the evaluated nuclear data file ENDF presents interpolations of experimental data which are much closer to data as is seen here, but they cannot be extrapolated to targets away from those which are usable for measurements. Minor

actinides may be too short-lived to serve as targets, but still they may play an important role for the composition of used fuel.

The extension of the new ansatz to targets with nonzero spin needs additional caution as the transition to the observer's system in Eq. (24) assumes the rotational energy to increase with spin. Data for resonance spacings near S_n are observed with neutron capture by odd nuclei with an elevated spin of usually single particle nature. It is thus disputable to simply extend Eq. (24) to higher spin, even if one of the several propositions [eg09] for the spin cut off parameter σ_i or dispersion parameter σ is inserted. A related ambiguity emerges, when one of these is used to construct a formula for the spin dependence: $\rho(E_x, J) = S_\sigma(J) \cdot \rho(E_x)$; for neither factor a convincing model is available and an adjustment to bound level energies depends on the accidental choice of A and Z . The ansatz presented here for small J avoids this problem and further study is needed to overcome this limitation. To extend predictions for radiative neutron capture into regions away from stable nuclei global parameterizations for photon strength and level density are required – and the success of the combination of TLO to Eq. (24) in the comparison to respective data may induce detailed theoretical investigations.

XI. Conclusions.

Various spectroscopic informations presented over the years [ku72, st84, cl86, an93, wu91, to13] indicate triaxiality for a number of heavy nuclei. Admission of the breaking of axial symmetry, albeit often rather weak, also improves a global description of Giant Dipole Resonance (IVGDR) shapes by a triple Lorentzian (TLO) as introduced recently [ju08, ju10]. These add up to the TRK sum rule, when theoretical predictions for the A -dependence of pole energies from droplet model [my77] and spreading widths based on one-body dissipation [bu91] are used. Two additional effects – hitherto not emphasised as such – indicate a breaking of axial symmetry in nearly all of the heavy nuclei: With one global parameter the scheme proposed here reproduces observations for level densities in nuclei with $A > 50$ and $J = \frac{1}{2}$, when (a) the Fermi gas prescription is only used above a phase transition due to the critical temperature, (b) a pairing condensation energy is included in the backshift and (c) the collective enhancement due to symmetry breaking by triaxiality is included. Only a modest modification of the level density parameter $\tilde{\alpha}$ from its nuclear matter value is needed to fit resonance spacing data with a surprisingly small surface term – the only free parameter. Again only one global parameter suffices to fit to the shape of the IVGDR peak by a triple Lorentzian photon strength (TLO), somewhat improved as compared to the original proposal [ju08, ju10], well in accord to the TRK sum rule. It also predicts its low energy tail – without other modification than the addition of minor components – to match respective strength data as well as neutron capture cross sections taken for nuclei with $50 < A < 254$ in the energy range of unresolved resonances.

A combination of both points is easily performed by considering spherical and axial symmetry to be broken – for low excitation in accord to CHFB calculations [de10] and more easily understood for increasing excitation energy. Exact deformation parameters are unimportant for the tail of the E1-resonance as well as for the density of low spin states occurring in neutron capture by even targets as neither spin cut off nor moments of inertia are involved. Thus a combination of the photon strength parameterization to the novel

approximation for level densities leads to a prediction on absolute scale for neutron capture in the range of unresolved resonances – including Maxwellian average cross sections compiled recently [di10] for $\langle E_n \rangle = 30$ keV. Four points are stressed again:

1. Ad hoc assumptions on shapes and collective enhancement in previous calculations [ca09] of compound nuclear rates are replaced by a direct account for broken symmetries.
2. Doing so, the established procedure to predict level densities is improved such, that only one small parameter suffices to obtain agreement to data on absolute scale.
3. The low energy tail derived from the global triple Lorentzian (TLO) fit to IVGDRs is not modified by extra energy dependence.
4. The predictions for average radiative widths and Maxwellian cross sections are sensitive to two not fully controlled ingredients to the calculations: The state density $\omega_{qp}(0)$ near the ground state of the final nucleus and the low energy electric dipole strength induced by coupling its quadrupole and octupole modes. For these a global prediction appears impossible and for Figs. 7 – 31 values were used, which were derived as upper limits to experimentally determined data; an incorporation of local information will improve the predictions. The possible increase of n-capture yields by some amount was discussed [sa13] to be caused by additional ‘pygmy’ photon strength, eventually related to a vibration of excess neutrons against a core with $A = Z$, as predicted [mo71] to appear below $0.5 \cdot E_{IVGR}$ and an excess above TLO at higher energies near S_n may also be related to a vortical proton motion [ry89]. The respective study finds a rather weak influence of such ‘pygmy’ strength.

In conclusion: For clearly more than 100 spin-0 target nuclei with $A > 50$ resonance spacing data and average capture cross sections are well described by a global fit with only a small number of adjusted quantities, which turn out to be A -independent. This successful ansatz can be used as basis for detailed studies in specific regions of the nuclide chart and this promises reliable predictions for other compound nuclear reactions besides radiative capture. The breaking of axial symmetry in excited heavy nuclei is demonstrated here on the basis of experimental data published previously – and further study of the influence of broken axial symmetry in addition to existing theoretical hints to the importance of triaxiality [hi53, df58, da65, ku72, ha84, bu91, fr01, ia03, ma04, mo06, de10, ni14] is wanted, as still nuclear theory studies often prefer to assume axial symmetry *ad hoc*. This hope comes from the data analysis presented here showing that the global ansatz derived on the basis of broken axial symmetry and the dipole sum rule allows remarkably good predictions for radiative neutron capture in general with very few free fit parameters. An application is envisaged also outside the valley of stability – important for nuclear astrophysics and for the transmutation of nuclear waste.

Acknowledgements

This work is supported by the German federal ministry for education and research BMBF (02NUK13A) and by the European Commission within the 7th EU framework programme under ERINDA (FP7-269499) and through Fission-2013-CHANDA (project no. 605203). Intense discussions within these projects and with other colleagues, especially with Ronald Schwengner, Julian Srebnry and Hermann Wolter, are gratefully acknowledged.

References

- ah85 J. Ahrens, Nucl. Phys. A, 446, 229 (1985)
- al08 E. Algin et al., Phys. Rev. C 78, 054321 (2008)
- al56 K. Alder et al., Rev. Mod. Phys. 28 (1956) 432
- al77 L. Aldea et al., Z. Physik A 283, 391 (1977)
- an01 W. Andrejtscheff et al., Phys. Lett. B 506 (2001) 239
- an93 W. Andrejtscheff and P. Petkov, Phys. Rev. C 48, 2531 (1993); id., Phys. Lett. B 329 (1994) 1
- ar81 A. Arima and F. Iachello, Ann. Rev. of Nucl. and Part. Sc. 31 (1981) 75
- au70 G. Audit et al., Nucl. Instr, 79 (1970) 203
- ax62 P. Axel, Phys. Rev. 126, 671 (1962).
- ax70 P. Axel et al., Phys. Rev. C 2, 689 (1970).
- ba73 G.A. Bartholomew et al., Adv. Nucl. Phys. 7 (1973) 229
- ba77 H.W. Barz, I. Rotter and J. Höhn, Nucl. Phys. A 275 (1977) 111; R. Wünsch, priv. comm.
- be67 B.L. Berman et al., Phys. Rev. 162 (1967) 1098
- be68 H. Bergère et al., Nucl. Phys. A121, 463 (1968); id., Nucl. Phys. A133, 417 (1969)
- be74 H. Beil et al., Nucl. Phys. A 219, 61 (1974); id., Nucl. Phys. A 227, 427 (1974)
- be75 B.L. Berman and S.C. Fultz, Rev. Mod. Phys. 47 (1975) 713, cf. [ex12]
- be82 Z.W. Bell et al., Phys. Rev. C 25, 791 (1982)
- be86 B.L. Berman et al., Phys. Rev. C 34 (1986) 2201
- be87 B.L. Berman et al., Phys. Rev. C 36 (1987) 1286
- be95 F. Bečvář et al., Phys. Rev. C 52 (1995) 1278
- be07 G.F. Bertsch et al., Phys. Rev. Lett. 99, 032502 (2007)
- be11 R. Beyer et al., Int. J. of Mod. Phys. E 20 (2011) 431
- be14 M. Beard et al., Phys. Rev. C 90 (2014) 034619
- bi87 Y. Birenbaum, et al., Phys. Rev. C 36 (1987) 1293
- bj74 S. Bjørnholm, A. Bohr and B. Mottelson, Rochester-conf., IAEA-STI/PUB/347 (1974) 367; dto., IAEA-SM-174/205
- bo57 A. Bohr and B.R. Mottelson, Nucl. Phys. 4 (1957) 529; id., 9 (1959) 687
- bo75 A. Bohr and B. Mottelson, Nuclear Structure ch. 6, (New York 1975)
- bo81 T.J. Bowles et al., Phys. Rev. C24 (1981) 1940
- bo83 T.J. Boal, E.G. Muirhead and D.J.S. Findlay, Nucl. Phys. A 406 (1983) 257
- bo90 E. Bortolani and G. Maino, Phys. Rev. C 43 (1991) 353
- bo06 A. Borella et al., Nucl. Sci. Eng. 152 (2006) 1
- br00 B. A. Brown, Phys. Rev. Lett. 85, 5300 (2000)
- br57 D. Brink, Nucl. Phys. 4, 215 (1957); dto., Ph.D. thesis, Oxford ()
- bu57 E. M. Burbidge et al., Rev. Mod. Phys. 29, 547 (1957)
- bu72 F. R. Buskirk et al., Phys. Lett. B 42, 194 (1972)
- bu91 B. Bush and Y. Alhassid, Nucl. Phys. A 531 (1991) 27
- ca71 P. Carlos et al., Nucl. Phys. A172, 437 (1971)
- ca74 P. Carlos et al., Nucl. Phys. A219, 61 (1974); id., Nucl. Phys. A225, 171 (1974)
- ca79 R. Casten et al., Nucl. Phys. A 316 (1979) 61
- ca80 J.T. Caldwell et al., Phys. Rev. C 21 (1980) 1215
- ca09 R. Capote et al., Nucl. Data Sheets 110 (2009) 3107; id., <http://www-nds.iaea.org/RIPL-3/>
- ch84 T. Chapuran et al., Phys. Rev. C 30, 54 (1984)
- ch91 M.B. Chadwick et al., Phys. Rev. C 44, 814 (1991)
- ch06 M.B. Chadwick et al., Nucl. Data Sheets, 107, 12, 2931 (2006)

- cl86 D. Cline, Ann. Rev. Nucl. Part. Sci. 36 (1986) 683
- da58 M. Danos, Nucl. Phys. 5 (1958) 23
- da64 M. Danos and W. Greiner, Phys. Rev. 134, B 284 (1964)
- da65 J.P. Davidson, Rev. Mod. Phys. 37, 105 (1965)
- de10 J.-P. Delaroche et al., Phys. Rev. C 81 (2010) 014303; ibid., supplemental material
- df58 A.S. Davydov and J.P. Fillipov, Nucl. Phys. A 8(58)237
- di88 S.S. Dietrich and B. L. Berman, At. Data and Nucl. Data Tables 38, 199 (1988) ; cf. [ex12]
- di10 I. Dillmann et al., Phys. Rev. C 81, 015801 (2010); id., AIP Conf. Proc. 819, 123; <http://www.kadonis.org>
- dj82 C. Djalali et al., Nucl. Phys. A 380 (1982) 42
- do72 C.B. Dover, R. H. Lemmer, and F. J. W. Hahne, Ann. Phys. (N.Y.) 70, 458 (1972).
- do82 B.S. Dolbilkin et al., Phys. Rev. C 25 (1982) 2225; T. Saito et al., Phys. Rev. C 28 (1983) 652
- eg09 T. von Egidy and D. Bucurescu, Phys. Rev. C 80 (2009) 054310
- en92 G. Enders et al., Phys. Rev. Lett. 69 (1992) 249
- en05 J. Enders et al., Phys. Rev. C 71, 014306 (2005)
- en09 J. Endres et al., Phys. Rev. C 80, 034302 (2009), id., Phys. Rev. Lett. 105 (2010), 212503
- er10 M. Erhard et al, Phys. Rev. C 81, 034319 (2010)
- er60 T. Ericson, Advances in Physics, 9 (1960), 425, dto., Nucl. Phys. 6 (1958) 62
- es97 L. Esser et al., Phys. Rev. C 55 (1997) 206
- ex14 NNDC database: <http://www.nndc.bnl.gov/exfor/exfor00.htm> and ...exfor/endf00.jsp
- fi83 D.J.S. Findlay, Nucl. Instr. 213 (1983) 353
- fi86 C. Fiolhais, Annals of Physics, 171 (1986) 186
- fo06 L. Fortunato, S. De Baerdemacker, and K. Heyde, Phys. Rev. C 74, 014310 (2006)
- fr01 S. Frauendorf, Rev. Mod. Phys. 73, 463 (2001)
- fu69 S.C. Fultz et al., Phys. Rev. 186 (1969) 1255
- fu73 W. Furman et al., Phys. Lett. B 44 (1973) 465
- ge54 M. Gell-Mann et al., Phys. Rev. 95 (1954) 1612
- gi65 A. Gilbert and A. G. W. Cameron, Can. Journ. of Physics, 43 (1965) 1446
- gi82 M. Girod and B. Grammaticos, Phys. Rev. C 27 (1982) 2317
- go48 M. Goldhaber and E. Teller, Phys. Rev. 74 (1948) 1046
- go77 E.F. Gordon and R. Pitthan, Nucl. Inst. and Meth. 145 (1977) 569
- go78 A.M. Goryachev and G.N. Zalesny; Sov. J. Nucl. Phys. 27 (1978) 779, from Yad. Fiz. 27 (1978) 1479
- go98 K. Govaert et al., Phys. Rev. C 57 (1998) 2229
- gr85 M.K. Grossjean and H. Feldmeier, Nucl. Phys. A 444 (1985) 113.
- gr03 C. Granja et al., Nuclear Physics A 724 (2003) 14
- gr11 E. Grosse et al., Eur. Ph. Journ. WoC. 21, 04003 (2012); dto., 8, 02006 (2010)
- gr12 E. Grosse and A.R. Junghans, Landolt-Börnstein, New Series (2012) I/25D, 4
- gr14 E. Grosse, A.R. Junghans and R. Massarczyk, Phys. Lett. B 739 (2014) 1
- gu76 G.M. Gurevich et al., Nucl. Phys. A 273, 326 (1976)
- gu81 G.M. Gurevich et al., Nucl. Phys. A 351, 257 (1981)
- gu05 M. Guttormsen et al., Phys. Rev. C 71, 044307 (2005)
- gu12 M. Guttormsen et al., Phys. Rev. Lett 109, 162503 (2012)
- gu14 M. Guttormsen et al., Phys. Rev. C 89, 014302 (2014)
- gu15 M. Guttormsen et al., arXiv 1503.03300 (2015); cf. refs. given there
- gy98 S. Goriely, Phys. Lett. B 436 (1998) 10
- gy04 S. Goriely, E. Khan, and M. Samyn, Nucl. Phys. A739, 331 (2004)
- ha84 A. Hayashi, K. Hara and P. Ring, Phys. Rev. Lett. 53 (1984) 337
- ha90 P. G. Hansen, B. Jonson, and A. Richter, Nucl. Phys. A 518, 13 (1990)

- ha02 I. Hamamoto and H. Sagawa, Phys. Rev. C 66, 044315 (2002)
- he07 M. Herman et al., Nucl. Data Sheets. 108 (2007) 2655; id., www.nndc.bnl.gov/empire
- he10 K. Heyde et al., Rev. Mod. Phys. 82, 2365 (2010)
- hi53 D.L. Hill and J.A. Wheeler, Phys. Rev. 89 (1953) 1102
- ho91 S.D. Hoblit and A.M. Nathan, Phys. Rev. 44 (1991) 2372
- hu74 J. R. Huizenga et al., Nucl. Phys. A 223 (1974) 589
- ia03 F. Iachello, Phys. Rev. Lett. 91 (2003) 132502
- ig93 A. Ignatyuk et al., Phys. Rev. C 47 (1993) 1504
- ig06 A. Ignatyuk, RIPL-3, IAEA-TECDOC-1506 (2006); www-nds.iaea.org/RIPL-3/resonances
- is04 B. S. Ishkhanov and V. V. Varlamov, Physics of Atomic Nuclei 67 (2004) 1664
- is13 J. Isaak et al., Phys. Lett. B 727 (2013) 361
- jo07 J. Joly, Progress in Particle and Nuclear Physics 59 (2007), 337
- ju95 A. Jung et al., Nucl. Phys. A 584 (1995) 103
- ju98 A.R. Junghans et al., Nucl. Phys. A 629 (1998) 635; *ibid.*, A649 (1999) 214c
- ju08 A.R. Junghans et al., Phys. Lett. B 670 (2008) 200
- ju10 A.R. Junghans et al., Journ. Korean Phys. Soc. 59, 1872 (2010)
- ka78 S.K. Kataria, V. S. Rarnamurthy, and S. S. Kapoor, Phys. Rev. C 18 (1978) 549
- ka83 S.G. Kadmeneskii, V.P. Markushev and V.I. Furman, Sov. J. Nucl. Phys. 37 (1983) 165
- ka89 F. Käppeler et al., Rep. Progr. Phys. 52, 945 (1989)
- ka11 F. Käppeler et al., Rev. Mod. Phys., 83 (2011) 157
- ki80 T. Kibédi and R. Spear, At. Data and Nucl. Data Tables 80, 35 (2002)
- kn95 U. Kneissl et al., Progr. in Part. and Nucl. Phys. 34 (1995) 285, *ibid.*, 37 (1996) 349
- kn06 U. Kneissl et al., J. Phys. G 32 (2006) R217
- ko90 J. Kopecky and M. Uhl, Phys. Rev. C 41, 1941 (1990) and previous work quoted there
- ko05 C. Kohstall et al., Phys. Rev. C 72 (2005) 034302
- ko08 A. Koning et al., Nucl. Phys. A 810 (2008) 13; *dto.*, www.talys.eu
- kr04 M. Krticka et al., Phys. Rev. Lett. 92 (2004) 172501
- kr13 J. Kroll et al., Phys. Rev. C 88, 034317 (2013)
- ku25 W. Kuhn, Zeitschr. f. Phys. 33, 408 (1925); F. Reiche and W. Thomas, Zeitschr. f. Phys. 34, 510 (1925)
- ku72 K. Kumar, Phys. Rev. Lett. 28 (1972) 249
- ku81 G. Kühner et al., Phys. Lett. B104, 189 (1981)
- la57 A.M. Lane and J. E. Lynn, Proc. Phys. Soc. (London) A 70 (1957) 557
- la64 L.D. Landau and E.M. Lifschitz, Statistical Physics, 2nd. Ed., Moscow (1964), § 80
- la73 S.E. Larsson, Physica Scripta, 8 (1973) 17
- la79 R.M. Laszewski and P. Axel, Phys. Rev. C 19 (1979) 342
- la87 R.M. Laszewski et al., Phys. Rev. Lett. 59 (1987) 431
- la10 A. C. Larsen and S. Goriely, Phys. Rev. C 82 (2010) 014318
- le71 A. Leprêtre et al., Nucl. Phys. A 175, 609 (1971)
- le74 A. Leprêtre et al., Nucl. Phys. A 219, 39 (1974)
- le50 J. Levinger and H.A. Bethe, Phys. Rev. 78 (1950) 115
- li09 Z. P. Li et al., Phys. Rev. C 79, 054301 (2009), and references therein
- ma61 C.A. Mallmann, Nucl. Phys. 24 (1961) 535
- ma84 G. Maino et al., Phys. Rev. C 30 (1984) 2101
- ma04 A. Maj et al., Nucl. Phys. A 731 (2004) 319
- ma05 J.A. Maruhn et al., Phys. Rev. C 71(2005) 064328
- ma12 R. Massarczyk, et al., Phys. Rev. C 86, 014319 (2012); *dto*, private communication
- ma14 R. Massarczyk, et al., Phys. Rev. Lett. 112 (2014) 072501

- me74 J. Meyer-ter-Vehn, et al., Phys. Rev. Lett. 32 (1974) 383
- me94 A. Mengoni and Y. Nakajima, J. Nucl. Sci. & Technol. 31 (1994) 151
- mo06 P. Möller et. al., Phys. Rev. Lett. 95, 062501 (2006); id. At. Data and Nucl. Data Tables 94 (2008) 758
- mo71 R. Mohan, M. Danos and L. C. Biedenharn, Phys. Rev. C 3 (1971) 1740
- mo95 P. Möller et. al., At. Data and Nucl. Data Tables 59, 185 (1995)
- mo12 L.G. Moretto et al., Phys. Rev. C 86 (2012) 021303
- mo15 L.G. Moretto et al., Journal of Physics 580 (2015) 012048
- mu98 S.F. Mughabghab, C. Dunford, Phys. Rev. Lett. 81 (1998) 4083
- mu00 S.F. Mughabghab, C. Dunford, Phys. Lett. B 487 (2000) 155.
- my67 W.D. Myers and W.J. Swiatecki, Ark. Fizik 36 (1967) 343.
- my77 W. Myers et al., Phys. Rev. C 15 (1977) 2032
- na65 O. Nathan and S.G. Nilsson; α, β, γ -ray spectroscopy, K. Siegbahn ed., North Holland 1965
- na91 A.M. Nathan, Phys. Rev. C 43 (1991) 2479
- na08 C. Nair et al., Phys. Rev. C 78, 055802 (2008)
- na10 C. Nair et al., Phys. Rev. Phys. Rev. C 81, 055806 (2010)
- ni14 T. Nikšić, P. Marević, and D. Vretenar, C 89 (2014) 044325 and refs. quoted there
- no78 J.W. Norbury et al., Aus. Journ. of Phys. 31, 471 (1978)
- oe14 B. Oezel-Tashenov et al., Phys. Rev. C 90 (2014) 024304
- ok12 Y. Oktem et al., Phys. Rev. C 86, 054305 (2012)
- pe01 J.M. Pearson, Hyp. Int 132, 2001, 59
- pi74 R. Pitthan et al., Phys. Rev. Lett. 33 (1974) 849; id., Phys. Rev. 21 (1980) 28
- pi94 N. Pietralla et al., Phys. Rev. Lett. 73, 2962 (1994)
- pi09 N. Pietralla et al., Phys. Lett. B 681 (2009) 134
- pl11 V.A. Plujko et al., At. Data and Nucl. Data Tables 97 (2011) 567; <http://www-nds.iaea.org/RIPL-3/gamma>
- po72 Yu.P. Popov et al., Nucl. Phys. A 188 (1972) 212; id., Sovj. Journ. of Part. and Nuclei, 13 (1982) 483
- po73 K. Pomorski et al. , Nucl. Phys. A205 (1973) 433
- po75 W. Poenitz, Nucl. Sci. Eng. 57 (1975) 300
- po92 T.D. Poelhekken et al., Phys. Lett. B 278 (1992) 423
- pr10 B. Pritychenko et al., At. Data and Nucl. Data Tables 96 (2010) 645; www.nndc.bnl.gov/astro
- ra01 S. Raman et al., At. Data and Nucl. Data Tables 78 (2001) 1
- ro57 H. Rose, J. Nuclear Energy 5, 4 (1957)
- ro11 L. M. Robledo and G. F. Bertsch, Phys. Rev. C 84, 054302 (2011)
- ro13 C. Romig et al., Phys. Rev. C 88 (2013) 044331
- ru08 G. Rusev et al., Phys. Rev. C 77 (2008) 064321; id., Phys. Rev. C 79 (2009) 061302
- ru09 G. Rusev et al., AIP Conf. Proc. 1099, 799 (2009); <http://link.aip.org/link/doi/10.1063/1.3120158>
- ru13 G. Rusev et al., Phys. Rev. Lett. 110 (2013) 022503; id., Phys. Rev. C 87 (2013) 054603
- ry89 N. Ryezayeva et al., Phys. Rev. Lett. 89, 272502
- sa11 M. Salvatores and G. Palmiotti, Prog. Part. Nucl. Phys. 66, 144 (2011)
- sa13 D. Savran et al., Prog. Part. Nucl. Phys. 70 (2013) 210; id., Phys. Rev. Lett. 100 (2008) 232501
- sa14 A. Sauerwein et al. Phys. Rev. C 89, 035803 (2014)
- sc35 H. Schiller u. Th. Schmidt, Zeits. f. Phys. 94 (1935) 457, id., 95 (1935) 265; id., 98 (1936) 430,
- sc75 A. Schwierczinski et al., Phys. Rev. Lett. 35 (1975) 1244
- sc88 R. Schwengner et al., Nucl. Phys. A 486 (1988) 43; id. Nucl. Phys. A 509 (1990) 550
- sc07 R. Schwengner et al., Phys. Rev. C 76 (2007) 034321; id., Phys. Rev. C 78, 064314 (2008)
- sc10 R. Schwengner et al., Phys. Rev. C 81, 054315 (2010)
- sc11 G. Schramm et al., Phys. Rev. C 85 (2011) 014311
- sc13 R. Schwengner, S. Frauendorf, and A. Larsen, Phys. Rev. Lett. 111 (2013) 232504

- se74 R. Sedlmayr, M. Sedlmayr and W. Greiner, Nucl. Phys. A 232 (1974) 465
- si06 A. Schiller et al., Phys. Lett. B 633 (2006) 225
- so12 A. Sonzogni, (2012); www.nndc.bnl.gov/nudat2/indx_adopted.jsp
- sp75 R.R. Spencer and F. Kaeppler, Wash. conf. 2 (1975) 620
- sr06 J. Srebnry et al., Nucl. Phys. A **766** (2006) 25; id., Int. J. of Mod. Phys. E 20 (2011) 422 and refs. quoted therein.
- st50 H. Steinwedel and H. Jensen, Phys. Rev. 79 (1950) 1019
- st84 J. Stachel et al., Nucl. Phys. A 419 (1984) 589; id. Nucl. Phys. A 383 (1982) 425
- st05 N.J. Stone, At. Data and Nucl. Data Tables 90 (2005) 75
- t013 Y. Toh et al., Phys. Rev. C 87 (2013) 041304
- to10 A. P. Tonchev et al., Phys. Rev. Lett. 104, 072501 (2010)
- ul87 J. L. Ullmann et al., Phys. Rev. C 35 (1987) 1099; id., (2014)
- ut08 H. Utsunomiya et al., Phys. Rev. Lett. 100, 162502 (2008)
- ut10 H. Utsunomiya et al., Phys. Rev. C 81, 035801 (2010); id., Phys. Rev. C 82, 064610 (2010)
- ut11 H. Utsunomiya et al., Phys. Rev. C 84, 055805 (2011)
- ut13 H. Utsunomiya et al., Phys. Rev. C 88, 015805 (2013)
- va69 O.V. Vasilyev et al., Sovj. Journ. Nucl. Phys., 13, 259 (1969); *id.*, Yadernaja Fizika 13, 463 (1971)
- va04 V.V. Varlamov et al., J. Phys. Atom. Nucl., 67 (2004) 2107; *ibid.* 75 (2012) 1339
- va14 V.V. Varlamov et al., Eur. Phys. J. A 50 (2014) 114
- vc84 E. Van Camp et al., Phys. Rev. C 30 (1984) 1182
- ve70 A. Veyssi  re et al., Nucl. Phys. A159, 561 (1970); *ibid.* A 199, 45 (1973); *id.*, Journal de Physique 36 (1975) L267, cf. [di88]
- vi82 S.E. Vigdor and H.J. Karwowski, Phys. Rev. C 26 (1982) 1068
- vo04 A. Voinov et al., Phys. Rev. Lett. 93, 142504 (2004)
- vy78 R. Van de Vyver et al., Zeitschr. f. Phys. A 284, 91 (1978)
- we73 W. Weise, Phys. Rev. Lett. 31 (1973) 773
- we77 L.W. Weston and J.H. Todd, Nucl. Sci. Eng. 63, (1977) 143
- we80 H.R. Weller and N.R. Roberson, Rev. Mod. Phys. 52 (1980) 699; H.R. Weller et al., Prog. in Part. & Nucl. Ph. 62 (2009) 257
- we05 V. Werner et al., Phys. Rev. C 71, 054314 (2005)
- wi01 K. Wissak, F. Voss, F. Kaeppler, Nucl. Sci. Eng. 137 (2001) 183
- wo91 A. van der Woude, Progr. in Part. and Nucl. Phys. 18 (1987) 217 in Electr. and Magn. Giant Res., J. Speth Ed. (1991)
- wr12 K. Wrzosek-Lipska et al., PRC 86, 064305 (2012)
- wu91 C. Y. Wu et al., Nucl. Phys. A 533 (1991) 359; *id.*, Nucl. Phys. A 607 (1996) 178
- wu96 C. Y. Wu and D. Cline, Phys. Rev. C 54 (1996) 2356
- yo04 D.H. Youngblood et al., Phys. Rev. C 69, 034315 (2004)
- zh09 S. Q. Zhang et al., Phys. Rev. C 80, 021307 (2009)
- zi02 M. Zielinska et al., Nucl. Phys. A 712 (2002) 3
- zi05 A. Zilges et al., Progr. in Part. and Nucl. Phys. 55 (2005) 408, *id.*, AIP Conference Proceedings 831 (2006) 147